

The HI Content of Spirals. II. Gas Deficiency in Cluster Galaxies

José M. Solanes

Departament d'Enginyeria Informàtica i Matemàtiques, Universitat Rovira i Virgili. Carretera de Salou, s/n; E-43006 Tarragona, Spain

`jsolanes@etse.urv.es`

Alberto Manrique

Departament d'Astronomia i Meteorologia, Universitat de Barcelona. Av. Diagonal 647; E-08028 Barcelona, Spain

`Alberto.Manrique@am.ub.es`

Carlos García-Gómez

Departament d'Enginyeria Informàtica i Matemàtiques, Universitat Rovira i Virgili. Carretera de Salou, s/n; E-43006 Tarragona, Spain

`cgarcia@etse.urv.es`

Guillermo González-Casado

Departament de Matemàtica Aplicada II, Universitat Politècnica de Catalunya. Pau Gargallo 5; E-08028 Barcelona, Spain

`guille@ma2.upc.es`

and

Riccardo Giovanelli and Martha P. Haynes

*Center for Radiophysics and Space Research and National Astronomy and Ionosphere Center,¹
Cornell University; Ithaca, NY 14853*

`(riccardo,haynes)@astrosun.tn.cornell.edu`

ABSTRACT

We derive the atomic hydrogen content for a total of 1900 spirals in the fields of eighteen nearby clusters. By comparing the HI deficiency distributions of the galaxies inside of and outside of one Abell radius (R_A) of each cluster, we find that two thirds of the clusters in our sample show a dearth of neutral gas in their interiors. Possible

connections between the gaseous deficiency and the characteristics of both the underlying galaxies and their environment are investigated in order to gain insight into the mechanisms responsible for HI depletion. While we do not find a statistically significant variation of the fraction of HI-deficient spirals in a cluster with its global properties, a number of correlations emerge that argue in favor of the interplay between spiral disks and their environment. In the clusters in which neutral gas deficiency is pronounced, we see clear indications that the degree of HI depletion is related to the morphology of the galaxies and not to their optical size: early-type and, probably, dwarf spirals are more easily emptied of gas than the intermediate Sbc–Sc types. Gas contents below one tenth, and even one hundredth, of the expectation value have been measured, implying that gas removal is very efficient. The radial extent of the region with significant gas ablation can reach up to $2R_A$. Within this zone, the proportion of gas-poor spirals increases continuously towards the cluster center. The wealth of 21-cm data collected for the Virgo region has made it possible to study the 2D pattern of HI deficiency in that cluster. The map of gas deficiency in the Virgo central area points to an scenario in which gas losses result from the interaction of the disks with the inner hot intracluster gas around M87. We also find evidence that gas-poor spirals in HI-deficient clusters move on orbits more radial than those of the gas-rich objects. The implications of all these results on models of how galaxies interact with their environment are reviewed. Hydrodynamic effects appear as the most plausible cause of HI removal.

Subject headings: galaxies: clusters: general — galaxies: evolution — galaxies: ISM — galaxies: spiral — methods: data analysis — radio lines: galaxies

1. Introduction

In nearby clusters, environmental interactions leave their imprint on the fragile gaseous disks of the spirals. As a result, comparison of the neutral hydrogen content of cluster objects with respect to their field counterparts has been frequently used to evaluate the strength of these perturbations and to identify their physical origin. Thus far, the most extensive 21-cm-line studies of high galaxian density regions have been those of Giovanelli & Haynes (1985, hereinafter GH85), who examined a sample of nine nearby clusters, and those reported by Haynes & Giovanelli (1986, hereinafter HG86) and Hoffman, Helou, & Salpeter (1988), who investigated large compilations of Virgo cluster galaxies. The HI data published by R. G. and M. P. H. have been analyzed further by Dressler (1986), Magri et al. (1988), and Valluri & Jog (1991). These investigations argued in favor

¹The National Astronomy and Ionosphere Center is operated by Cornell University under a cooperative agreement with the National Science Foundation.

of an ongoing interaction between spiral disks and their environment, but the process responsible for the gas depletion could not be unambiguously identified.

Because of the renewed interest in the interplay between galaxies and their surroundings and the substantial body of new cluster HI data that have been accumulated, conditions are ripe for a new evaluation of the HI content of galaxies in clusters that can provide fresh input to the debate about the extent to which the environment influences the evolution of galaxies. The first steps in this direction were taken a few years ago in a paper by Solanes, Giovanelli, & Haynes (1996, hereinafter Paper I), which was focused on the derivation of Malmquist-bias free estimates of the HI mass standards for the different morphological subgroups of luminous spirals. In the present paper, we exploit a large dataset of HI observations of spiral galaxies in the regions of eighteen nearby clusters with the aim of unmasking the cause of the observed gas deficiency.

The outline of the paper is as follows. The next section describes the criteria adopted for the selection of the cluster galaxy samples and the manner in which the HI deficiency is measured. The Virgo cluster and a composite formed by the remaining HI-deficient systems are used in § 3 to investigate the spatial pattern of HI deficiency. The dependence of HI deficiency both on the main global properties of clusters, and on the morphology and size of the galaxies is explored in § 4 and 5, respectively. Finally, § 6 examines the orbits of the spirals in HI-deficient clusters according to their gaseous content. The implications of the results of such analyses are discussed in § 7. The paper concludes with a summary of our findings. For all calculations involving the Hubble parameter we take $H_0 = 100 h \text{ km s}^{-1} \text{ Mpc}^{-1}$.

2. The Cluster Sample

The galaxies used in the present study have been extracted from the all-sky database of nearby galaxies maintained by R. G. and M. P. H. known as the Arecibo General Catalog (AGC). Apart from several entries listing 21-cm line information, the AGC contains an extensive compilation of galaxy parameters from optical observations, such as morphologies and apparent sizes. A large number of galaxies have morphological types and visual estimates of their angular diameters listed in the *Uppsala General Catalog of Galaxies* (UGC, Nilson 1973). For non-UGC objects, these properties have been obtained from the visual examination of the Palomar Observatory Sky Survey prints. The typical uncertainty in the morphological classification is $+/-$ one Hubble type, although for some individual galaxies, especially the ones with the smallest angular sizes, the errors may be larger. Apparent diameters are estimated in bins of $0'.1$ for dimensions larger than $1'$ and in bins of $0'.05$ for dimensions below that value. Because the eye measures at about the level of a *face-on* isophotal radius, independently of inclination (Giovanelli et al. 1994), visual diameters have not been corrected for the inclination of the parent galaxy (internal absorption). We also neglect the effects of galactic extinction on apparent dimensions. The AGC also contains information on heliocentric radial velocities from radio and/or optical wavelengths (the radio measurement taking always preference over the optical one when the two are available).

Following our previous work in this subject, HI deficiencies for individual galaxies have been quantified by means of a parameter DEF that compares, in logarithmic units, the observed HI mass, $h^2 M_{\text{HI}}^{\text{obs}}$, inferred from the corrected HI flux, with the value expected from an isolated (i.e. free from external influences) galaxy of the same morphological type, T^{obs} , and optical linear diameter, $h D_{\text{opt}}^{\text{obs}}$, calculated from the major visual dimension (for details, see Haynes & Giovanelli 1984, hereinafter HG84). Specifically:

$$\text{DEF} = \langle \log M_{\text{HI}}(T^{\text{obs}}, D_{\text{opt}}^{\text{obs}}) \rangle - \log M_{\text{HI}}^{\text{obs}}, \quad (1)$$

so positive values of DEF indicate HI deficiency. In eq. (1) the HI mass is expressed in solar units and the optical diameter in kpc. For the expectation value of the (logarithm of the) HI mass, we use the maximum likelihood linear regressions of $\log(h^2 M_{\text{HI}})$ on $\log(h D_{\text{opt}})$ inferred from the field galaxy sample summarized in Table 2 of Paper I. Because the standards of normalcy for the HI content are well defined only for the giant spiral population (Sa–Sc), we have excluded from the present study earlier Hubble types, as well as all galaxies unclassified or with peculiar or very disturbed morphologies. Nonetheless, HI mass contents for the few HI-rich Sd’s, Sdm’s, and Magellanic-type irregulars included in our samples have been calculated from the relationship inferred for the Sc’s following the results of HG84. Because the AGC data have been gathered from a wide variety of sources, data quality is inhomogeneous. While we have been careful to select only those galaxies for which a meaningful HI measure can be calculated, the reader should be aware that the applicability of the assembled dataset is essentially statistical. Imprecisions in the diameter measures and morphological type assignments, together with the built-in distance dependence of the $M_{\text{HI}} - D_{\text{opt}}$ relationship, make determinations of the HI deficiency for individual objects uncertain.

To be assigned to a given cluster field, a galaxy must lie within a projected distance of $5R_A$, i.e. within $7.5 h^{-1}$ Mpc, of the cluster center and have a radial velocity which is separated from the recessional velocity of the cluster no more than ~ 3 times its average velocity dispersion. Since we are especially interested in the central portions of clusters where environmental influences are strongest, we have only selected those clusters with at least 10 galaxies (of types Sa–Sdm/Irr) with good HI detections located within the innermost $1R_A$ ($1.5 h^{-1}$ Mpc) radius circle.

Of all the cluster fields sampled in the AGC a total of eighteen satisfy all the above constraints. These are the sky regions centered on the ACO (Abell, Corwin, & Olowin 1989) clusters A262, A397, A400, A426 (Perseus), A539, A779, A1060 (Hydra I), A1367, A1656 (Coma), A2063, A2147, A2151 (Hercules), and A3526 (Centaurus30), on the clusters of Virgo, Pegasus, Cancer, and Pisces, and on the group of galaxies around NGC507, hereinafter referred to as N507. Table 1 lists, for the above galaxy concentrations, the following quantities: cluster name in column (1); in columns (2) and (3) the cluster center coordinates referred to the 1950 epoch (mostly taken from the *Einstein* catalog of Jones & Forman 1999; when no X-ray observations are available—as for N507—we use the peak of the galaxy distribution); our velocity filter used to define cluster membership in column (4); in column (5) the Abell radius of the cluster expressed in degrees, inferred from its cosmological distance; and in columns (6) and (7), respectively, the total number of S’s meeting the membership

criteria within 1 and $5R_A$, except for the Virgo cluster region for which a maximum radial cutoff of $3R_A$ has been imposed to avoid dealing with large angular separations. The sky distributions of the galaxies belonging to each one of the eighteen cluster regions are plotted in Figure 1. Figure 2 shows the histograms of the distribution of the measured values of DEF according to equation (1) for these same regions. In the histograms, the filled areas illustrate the distribution for the galaxies within $1R_A$ —for which we adopt the cluster distance—, while the unfilled areas correspond to those objects at larger radii. Apart from some expected contamination by outliers, it is evident from this latter figure that, while the outer distributions tend to be bell-shaped, exhibit a dispersion comparable to the value of 0.24 measured for isolated galaxies (see Paper I), and peak around zero DEF, the central galaxies of the majority of the clusters show evidence for strong HI deficiency. The most notable case is that of Virgo, for which some of the inner galaxies have HI masses up to two orders of magnitude below their expectation values. Note that some of the datasets include a few galaxies undetected in HI but for which a reliable upper limit of their HI content has been calculated (see again HG84 for further details). In the calculations of DEF made through this paper, non-detections always contribute with their nominal lower limit of deficiency.

We choose to define a cluster as HI deficient when a two-sample Kolmogorov-Smirnov (KS) test gives a probability of less than 10% that its observed inner and outer distributions of DEF are drawn from the same parent population. Although it could be argued that the small size of the inner distributions makes some comparisons uncertain, the adopted definition has the advantage of being fully objective. Indeed, the results of the KS test confirm essentially the visual impression: the central spiral populations of twelve of the cluster fields in our dataset, Pegasus, Virgo, A262, A397, A400, A426, A779, A1060, A1367, A1656, A2063, and A2147 (identified in Fig. 2 by an asterisk after the name) have statistically significant reduced HI contents. Among these, only for A400 and A1060—two clusters with rather complex central velocity distributions (see e.g. Beers et al. 1992; Fitchett & Merrit 1988)— is it not possible to reject the null hypothesis at better than the 5% level of significance. For the other six galaxy concentrations, Cancer, N507, Pisces, A539, A2151, and A3526, the presence of objects with large HI deficiencies in the central regions is an exception of the norm. The results of the KS test are listed in the last column of Table 1.

From Figure 2 and Table 1, it is also readily apparent that, in spite of the stricter radial cutoff applied, the galaxy sample of the Virgo region is, because of its proximity, the largest. The difference in size is especially striking when one looks at the central $1R_A$ -radius circle: within this zone, clusters other than Virgo contain on the average 20 objects, while this latter system has nearly 11 times more galaxies. Thanks to this substantial wealth of HI data, Virgo is the only single cluster of our dataset for which it is possible to investigate in detail the relationship of HI deficiency with the position, morphology and kinematics of the galaxies (see §§ 3.1, 5, and 6). The remaining galaxy samples are useful to investigate the HI deficiency only in an overall sense, while for more detailed analysis, one must resort to the combination of the individual datasets to increase the statistical reliability of the results.

3. The Spatial Pattern of HI Deficiency

3.1. The Virgo Cluster

The Virgo cluster is the nearest large-scale galaxy concentration which offers the possibility of exploring the manifestations of environmental effects on galaxies with greatest detail. Nowadays, thanks to the large amount of 21-cm data accumulated, the case supporting the HI deficiency of the spirals in the core of this cluster is solidly established (e.g. Davis & Lewis 1973; van den Bergh 1976; Giovanardi et al. 1983; Giovanelli & Haynes 1983; Chamaraux, Balkowski, & Fontanelli 1986; HG86; Guiderdoni 1987). It has also been clearly demonstrated that the sizes of the gaseous disks of the HI-poor Virgo spirals are reduced with respect to their field counterparts (e.g. Helou et al. 1981; Giovanardi et al. 1983; Giovanelli & Haynes 1983; Warmels 1988a,b) in an amount that increases with decreasing distance to the cluster center—marked by the giant elliptical galaxy M87 (Warmels 1986; Cayatte et al. 1994). The selective sweeping of HI in the outer portions of the disks points to gas removal mechanisms initiated by the surrounding intergalactic medium (IGM).

Figure 3 shows the 2D adaptive map of the gas deficiency in the central cluster region. We have restricted our original Virgo sample to the subset of 187 galaxies with good 21-cm measures located in a region of size $10^\circ \times 10^\circ$ bounded by $12^{\text{h}}7^{\text{m}} \leq \text{R.A.} \leq 12^{\text{h}}47^{\text{m}}$, $6^\circ5 \leq \text{Dec.} \leq 16^\circ5$. This region is centered on (and covers most of) the classical Virgo I Cluster area (de Vaucouleurs & de Vaucouleurs 1973). When constructing the HI-deficiency map, we have also taken into account the close proximity and dynamical complexity of the Virgo cluster. The lack of correspondence between the observed radial velocity and distance in regions detached from the Hubble flow is a source of scatter that, for the nearby Virgo system, largely dominates the calculation of intrinsic parameters that have a built-in distance dependence, such as our deficiency estimator (eq. [1]): $M_{\text{HI}} \propto D_{\text{opt}}^n$, with $n \approx 1.7$ for Sc’s and $n \approx 1.2$ for earlier spiral types (Paper I). To estimate the contribution to the HI-deficiency map of spurious fluctuations caused by possible erroneous distance assignments, we have derived a second map by using a distance-independent approximation to equation (1) based on the difference between the expected and observed logarithm of the mean HI surface density, $\bar{\Sigma}_{\text{HI}}$, that is:

$$\text{DEF} = \langle \log \bar{\Sigma}_{\text{HI}}(T^{\text{obs}}) \rangle - \log \bar{\Sigma}_{\text{HI}}^{\text{obs}} , \quad (2)$$

with $\bar{\Sigma}_{\text{HI}} = F_{\text{HI}}/a_{\text{opt}}^2$, and where F_{HI} represents the corrected HI flux density integrated over the profile width in units of Jy km s^{-1} and a_{opt} the apparent optical diameter in arcmin (see also eqs. [3], [6], and [7] of Paper I). Note that $\bar{\Sigma}_{\text{HI}}$ is a hybrid quantity since it uses the optical disk area. Figure 3 shows that, except for a global mild enhancement of ~ 0.15 units in the values of the HI deficiency parameter most likely caused by background contamination, the original radio map (Fig. 3a) exhibits a spatial distribution of deficiency almost identical to that of its distance-independent approximation (Fig. 3b). This result allow us to conclude that all the fluctuations depicted in the Figure 3a reflect true local variations in the gas content of the galaxies.

Several structures emerge clearly from the cluster HI deficiency distribution. The zone with the maximum gas deficiency coincides with both the peak of X-ray emission and the main density

enhancement known as Cluster A (Binggeli, Popescu, & Tammann 1993). This is a double system comprising the subclusters centered on the giant ellipticals M87 and M86, which seem to be in the process of merging (Schindler, Binggeli, & Böhringer 1999). Five other distinct gas-deficient patches appear to be radially connected with the central one. Two of them are located along the N-S direction: to the South, the HI deficiency extends towards the clump dominated by M49 (Cluster B in Binggeli et al. 1993); to the North, there is a mild increase of gas deficiency around the spiral M100. Along the EW axis, the distribution of HI deficiency is dominated by a region of strong gas depletion to the East. This EW asymmetry in the HI content has also been observed at X-ray wavelengths by Böhringer et al. (1994), who found that the faint Virgo X-ray emission can be traced out to a distance of $\lesssim 5^\circ$, except in the western side where the emission falls off more steeply. On the other hand, the position of the eastern local maximum of deficiency is located about one and a half degrees South of the peak of the density enhancement known as Cluster C around the pair of galaxies M59 and M60. The last two zones of important HI depletion are found near the periphery of the surveyed region, where no X-ray gas is detected, in the areas of the background galaxy concentrations known as the M cloud in the NW, and the W' group and (northernmost part of the) W cloud in the SW.

We comment upon the implications of the maps depicted in Figure 3 on the possible origin of gas deficiency in this cluster at the end of § 7.

3.2. The Radial Variation of HI Deficiency

A well-known property of the HI deficiency pattern in clusters is its radial nature. Previous studies of cluster galaxy samples have already revealed that gas-poor objects are more abundant in the centers of clusters than in their periphery (Giovanelli, Chincarini, & Haynes 1981; Sullivan et al. 1981; Bothun, Schommer, & Sullivan 1984; GH85; HG86; Magri et al. 1988; Bravo-Alfaro et al. 2000). With our new data, this effect can also be observed in the greyscale maps depicting the HI deficiency distribution in the dynamically unrelaxed Virgo core (Fig. 3). In spite of the irregular distribution of the galaxies, the shade intensity of these maps, which is proportional to the deficiency measure, grows toward the position of M87, where the density of the environment is highest.

A more precise characterization of the radial behavior of HI deficiency is obtained by combining into a single dataset the HI measures for spirals in all the clusters which show HI deficiency other than Virgo (see § 2), with their clustercentric distances normalized to R_A . This composite sample of eleven HI-deficient clusters allows us to trace deficiency out to projected distances from the cluster center of $5R_A$ in much greater detail than the (relatively) small samples of the individual clusters, while at the same time reduces possible distortions caused by substructure and asphericity. Virgo is excluded from this composite cluster because of its smaller radial extent and the fact that its much larger dataset would dominate the composite cluster. Because the established upper limits of gas content for undetected galaxies in nearby clusters are more stringent than in distant ones, it is not

appropriate to use average values of DEF to characterize gas removal. We adopt instead a measure based on the relative populations of deficient and normal spirals, much less sensitive to the presence of censored data. In Figure 4, we show the variation in the fraction of spirals with $\text{DEF} > 0.30$ per bin of projected radial distance, in Abell radius units, for our composite HI-deficient cluster. The radial dependence of HI deficiency is clearly evident for $r \lesssim 2R_A$: the percentage of gas-poor spirals increases monotonically up to the center. Beyond this projected distance, however, the fraction of gas-deficient disks remains constant around a value of $\sim 10\text{--}15\%$, a value consistent with the fraction of field spirals with $\text{DEF} > 0.30$ expected from a Gaussian distribution of values of this parameter with an average dispersion of 0.24 (Paper I). Similar results are obtained when the deficiency threshold is increased to 0.48 (equivalent to a factor of three decrease in M_{HI}). We have also included in Figure 4 a second panel showing the variation of HI deficiency with projected radius. It provides visual verification of the fact that, at large clustercentric distances where gas-deficient galaxies are scarce and the contribution of non-detections negligible, the distributions of HI content at different radii are in excellent agreement both in terms of location and scale with that of field galaxies. This latter result supports further the statistical reliability of our measures of DEF through eq. (1).

The same two previous plots are repeated in Figure 5 for the superposition of the clusters which are not deficient in HI. It can be seen that the spirals belonging to these systems show HI contents which are both essentially independent of their clustercentric distance and typical of the field population. Comparison of the results in Figures 4 and 5 reinforce also our cluster subdivision into HI-deficient and “HI-normal” systems and therefore the soundness of the procedure followed for such classification.

It is clear from Figure 4 that the influence of the cluster environment on the neutral gas content of galaxies can extend beyond one Abell radius (plots of the radial variation of HI deficiency for individual clusters, not shown here, indicate that the extent of the zone of significant HI deficiency fluctuates significantly from cluster to cluster; see also GH85). On the other hand, Balogh et al. (1998), using [OII] equivalent width data, have found that the mean star formation rate in cluster galaxies, another property sensitive to environmental effects, shows signs of depression with respect to the field values at distances around twice the R_{200} “virial” radius². These results seem to pose a problem for stripping mechanisms which require high environmental densities to be effective. The reduction of both the gas content and the star formation rate of these outer cluster galaxies can be achieved, however, if they are on strongly eccentric orbits that have carried them through the cluster center at least once (see §§ 6 and 7). From the theoretical point of view, this possibility is supported by the simulations of hierarchical structure formation by Ghigna et al. (1998) and Ramírez & de Souza (1998), and by recent direct models of the origin of clustercentric gradients in

²In a typical nearby rich cluster the values of R_{200} and the Abell radius are similar: simple calculations show that these two scales coincide for a $z = 0$ cluster with a velocity dispersion of 866 km s^{-1} (Carlberg, Yee, & Ellingson 1997)

the star formation rates within cold dark matter cosmogonies by Balogh, Navarro, & Morris (2000).

4. HI Deficiency and Cluster Properties

The compilation of the principal properties of our clusters from the literature presents a number of difficulties, most important of which is the heterogeneity of the available data. Thus, in spite of the fact that for some of the clusters it is possible to draw their relevant parameters from detailed individual studies, data were extracted mainly from large cluster catalogs. By adopting this approach, we insure that the information available for each cluster property is homogeneous. The global parameters available for most of the systems in our sample are summarized in Table 2. These are: three different estimates of the X-ray luminosity in the 0.01–80 keV (bolometric), 0.5–3 keV (soft), and 2–10 keV (hard) bandpasses, in columns (2)–(4), respectively; spectral X-ray temperature (col. 5); radial velocity dispersion (col. 6); Abell galaxy number counts (col. 7); and spiral fraction (col. 8). Table 2 is completed with a global measure of the degree of gas removal in each cluster computed as the ratio of the number of spirals with $DEF > 0.30$ found within $1R_A$ of the cluster center to that of all objects of this type observed in HI within the same region. This “HI-deficient fraction”, F_{DEF} , and its associated Poissonian 1σ -error are indicated in column (9). The reference sources have been appended to the tabular information.

The fact that the characteristics of our clusters vary widely suggests that it is worth investigating correlations between the overall degree of gas depletion and the global cluster properties that reflect the strength of the environmental perturbations on the gaseous disks. Figure 6 shows the four X-ray parameters included in Table 2 plotted against F_{DEF} , while in Figure 7 this fraction is compared with the three optical properties. A fourth panel in this last figure compares the bolometric X-ray luminosity with the total spiral fraction. We note that all plots involving the parameter F_{DEF} resemble essentially scatter diagrams with no significant correlations. We have tested different thresholds of HI deficiency without finding appreciable changes. Neither does the use of the distance-independent approximation to DEF given by eq. (2) modify the results significantly, implying that the possible contamination by interlopers has a negligible contribution to the scatter of the relationships. Only for the Virgo cluster does the value of F_{DEF} drop significantly (from 63 to 46%), indicating that, for this system, most of the interlopers are located in the background.

We recall at this point that in the original investigation of GH85, suggestive though inconclusive indications of a trend toward greater HI-deficient fraction among clusters with high X-ray luminosity (in the 0.5–3.0 keV band) were found. This relationship, however, is not corroborated with the present larger dataset. One reasonable explanation for the lack of any discernible correlation is the possible transmutation of some of the swept spirals into lenticulars, thereby weakening the relationships we are investigating by reducing the fraction of HI deficient galaxies to a greater degree for the strong X-ray clusters than for the weak ones. This possibility is suggested by the very strong anticorrelation between the total spiral fraction and the X-ray luminosity ($r \leq -0.90$ for all three wavebands; see also Bahcall 1977 and Edge & Stewart 1991) in the bottom right panel

of Figure 7, implying that the fraction of lenticulars is correlated with X-ray luminosity.

One caveat that should be mentioned here is that possible selection effects and the incompleteness of some of our cluster galaxy samples—not included in the formal random error bars but which may blur significantly the results—might also explain the lack of good correlations between the fraction of HI-deficient spirals in clusters and the global properties of those systems. Note, for instance, that X-ray luminous clusters are more susceptible to incompleteness effects since they have a lower fraction of spirals. In an attempt to reduce the scatter of the plots, we have excluded from the analysis those samples containing fewer than 20 objects (identified in Figures 6 and 7 with light gray circles), which are the most likely affected by problems related to the small sample size. Systems in this restricted dataset certainly show signs of a possible relationship between F_{DEF} and the cluster X-ray luminosity in the 0.5–3.0 keV range (the linear correlation coefficient, r , is equal to 0.55), but there is no evidence for this trend in the other two X-ray windows. We argue that the results of the present exercise are not fully conclusive and require further investigation by means of still larger and more complete 21-cm-line investigation of galaxies in cluster fields.

5. HI Deficiency and Galaxy Properties

Important clues to the nature of HI deficiency can also be inferred from studying the variation of the degree of gas depletion with the intrinsic properties of the galaxies. In this section, we investigate possible connections between the gas content and the morphology and optical size of the disks.

5.1. Variation with Morphological Type

The increase of gas deficiency towards early morphological types was first noted for the Virgo giant spiral population by Stauffer (1983) and Guiderdoni & Rocca-Volmerange (1985). This trend was bolstered by Chamaraux et al. (1986), who found that the HI deficiency in the Virgo cluster spirals increases monotonically along the Hubble sequence from Sc to the earliest spiral types. GH85’s HI data were also found to obey a gas deficiency-morphology relationship by Dressler (1986), which was independent of the projected radial distance of the galaxies from the cluster center.

With our new, extensive data, the variation of HI deficiency with morphological type can now be reviewed in a far greater detail and put on a much firmer ground. We restrict the analysis to the twelve HI-deficient clusters to emphasize the significance of the results. As before, the data are grouped in a single composite cluster, except for the Virgo galaxies which are treated separately. We begin by presenting, in Figure 8, the bar charts of the percentage of galaxies inside $1R_A$ at a given morphology with deficiency parameter $\text{DEF} > 0.30$ in the Virgo and the composite samples. Hubble types have been replaced by its numerical T -code by HG84, which for the galaxies in the

present study runs from $T = 3$ for Sa’s to $T = 9$ for Sd–Sm and irregular galaxies. No distinction has been made between normal and barred spirals. Comparison of the two bar charts shows, in the first place, that the Virgo cluster exhibits a notably larger fraction of gas-deficient galaxies for any given morphological class, a result which is simply due to the fact that we are sampling farther down the HI mass function in Virgo than in the more distant clusters. Differences in the normalization aside, the bar charts confirm that for a spiral, the likelihood of being HI deficient depends on its morphology. Both the Virgo and the composite cluster sample share a common pattern: a roughly gradual descent of the fraction of HI-deficient galaxies as the Hubble type goes from Sa to Sc, by a total amount of $\sim 40\%$, which levels off for the latest types. The only discrepancy arises in the very latest morphology bin, which shows a noticeable recovery of the deficiency fraction for Virgo and a sharp drop for the composite cluster. In this case, we assign more credibility to the Virgo data since very gas-poor dwarf galaxies are underrepresented in the more distant clusters.

We have also produced for the above two cluster galaxy subsets the distributions of values of the parameter DEF separately by morphological type. Given the differences in the morphological composition between Virgo and the composite cluster (indicated by the numbers inside the bars in Fig. 8), we find it preferable to adopt a distinct type grouping for the two samples, so that we give priority to the reduction of statistical noise. A major feature of the plots displayed in Figure 9 is the strong positive skewness of all distributions. In the Virgo cluster, the Sa’s exhibit the most radical behavior: 16 out of the 21 galaxies of this type have HI deficiencies larger than 1, i.e. a factor of 10 decrement over the typical HI mass. Indeed, all Virgo galaxies with $\text{DEF} \geq 2$ belong to this subclass (it should be noted that the high fraction of non-detections for this type indicates even higher deficiency values than this limit). Most of the remaining strongly deficient galaxies ($\text{DEF} \geq 1$) in the Virgo sample, including the rest of the non-detections but one, belong to the Sdm/Irr class. This result demonstrates that the dwarf types, as well as the Sa’s, are not only more likely to be deficient in HI than the intermediate spirals, but they also have a higher gas deficiency. The distributions for the composite cluster, on the other hand, show a progressive increase in the positive skewness and boxiness towards the early types, but the differences among the histograms are less pronounced than for the Virgo data. There are also very few galaxies with $\text{DEF} \geq 1$. The fractions of non-detections, however, are seen to increase towards the two extremes of the morphological range. No doubt selection biases against galaxies with very low HI masses are responsible for the abrupt cutoff of the high-HI-deficiency tails of the distributions. Clearly, the Virgo sample is much deeper and complete than any of the other cluster galaxy samples under scrutiny.

Yet, the possibility remains that the observed correlation between HI deficiency and morphology might reflect nothing more than the well-known morphological segregation of cluster galaxies. In other words, the larger deficiency of the earlier types might be explained simply by their more central locations. Figure 10 demonstrates that this is not the case. In this plot, we reproduce the radial run of the HI-deficient fraction for the composite HI-deficient cluster sample of Figure 4 but separating the early ($T: 3 \div 6$) and late ($T: 7 \div 9$) spiral type subsets. From this graph, one

sees that, inside the region of influence of the cluster environment ($r \lesssim 2R_A$), early-type galaxies have systematically higher gas deficiencies, *at any projected radius*, than the late types. Identical results, although with more abrupt radial variations due to the spatial lumpiness of the cluster, are found for the Virgo sample. We can also rule out strong projection effects, which would affect preferentially the late types, for two reasons. The first argument results from the radial velocity filters applied in the selection of the galaxy samples. The second reason has to do with the fact that the contribution of a (presumably) uniform distribution of outliers would be less noticeable in the centermost radial bins, where the cluster density is the highest. Contrary to these expectations, Figure 10 shows that the difference between the HI-deficient fractions of the early- and late-type populations increases gradually towards the cluster center. We conclude that the observed correlation of HI deficiency and morphology is not a secondary effect of the spatial segregation of the galaxies, but reflects the interplay between the intrinsic characteristics of these objects and the physical mechanism behind HI depletion.

5.2. Variation with Galaxy Size

The analysis by Valluri & Jog (1991) of the central galaxies in four of the HI-deficient clusters identified by GH85—A262, A1367, Coma, and Virgo—revealed an apparent tendency for HI deficiency to increase with increasing optical galaxy size, a result arising essentially from the galaxies located at relatively large projected radial distances from the cluster center ($r > 0.75R_A$). According to those authors, this observational result was difficult to reconcile with galaxy-intracluster medium interactions, such as ram pressure stripping and transport processes, even if significant mass segregation was invoked. Therefore, it becomes quite important to review with our new data this possible relationship between optical size and gas deficiency, because its confirmation would put serious strain on some of the most popular mechanisms of gas depletion.

In order to emphasize the contribution of cluster members, we have restricted this study to the galaxies within a projected distance of $1R_A$ from the center of the twelve HI-deficient clusters identified in our catalog. The linear optical sizes of the galaxies are calculated from their major angular diameters as given in the AGC and from the mean cluster distances (see § 2). The optical diameters are then distributed in logarithmically spaced bins. As in previous sections, we have investigated separately the variation of the HI-deficient fraction as a function of galaxy size for the Virgo dataset and for the composite sample formed by the combination of the remaining HI-deficient clusters. The top two panels of Figure 11 depict the corresponding histograms. Contrary to the results reported in Valluri & Jog (1991), we find no obvious relationship between HI deficiency and optical size. A χ^2 -test corroborates that, statistically, there is no significant difference between the observed distributions and the uniform. We have verified that the results of the analysis are insensitive to alterations in the binning and to the exact deficiency criterion adopted.

We know from the results of the preceding sections that HI deficiency correlates with the morphology of the galaxies and their projected distance from the cluster center. As a simple method

of subtracting the contributions of these two factors to the correlation that is being investigated, we have broken down the original histograms by morphological type (EARLY or LATE) and radial position (INSide or OUTSide a circle of $r = 0.5R_A$). The results depicted, respectively, in the middle and bottom panels of Figure 11 correspond only to the Virgo cluster, but they can be extended to the composite cluster too. Inspection of these plots shows no noticeable differences between the behaviors of the histograms of each partition, which are all again statistically flat, except for the expected overall increase in the HI deficiency of the EARLY and IN subsets. Notice also that the dynamical range of the optical diameters for this dataset is much wider than that of the composite sample, justifying the independent analysis of the Virgo cluster.

Two arguments can be invoked to explain the different results obtained by Valluri & Jog (1991). The most important is the fact that the deficiency parameter adopted by those authors had a relatively strong residual dependence on the optical diameter, because it relied upon the comparison of the mean values of the hybrid surface density of HI (as in eq. [2]). As shown in Paper I, $\bar{\Sigma}_{\text{HI}}$ decreases significantly with increasing disk size for all the giant spiral types but the latest. Since the galaxy population in dense environments is biased against late disks, investigations of the HI deficiency in galaxy clusters based on the constancy of this quantity are likely to overestimate (underestimate) the gas deficiency of the largest (smallest) objects. At the time the earlier study was made, however, the standards of HI content available predicted that $M_{\text{HI}} \propto D_{\text{opt}}^{1.8}$ for the entire spiral population (HG84). This prompted Valluri & Jog to neglect the intrinsic size dependence of $\bar{\Sigma}_{\text{HI}}$ as insufficient to explain the observed trend. A second factor that might have contributed to generate the false relationship is the small size of the galaxy samples, which forced those authors to operate with a reduced number of intervals dominated by strong numerical uncertainties.

6. HI Deficiency and Galaxy Orbits

The hypothesis that HI-deficient galaxies lose their interstellar HI at small distances from cluster cores but can still be found at large radial distances (§ 3.2) suggests that the HI-deficient objects follow highly eccentric orbits. We now investigate the trajectories of the galaxies in the central regions ($r \leq 1R_A$) of Virgo and the composite HI-deficient cluster as a function of their gas contents and morphologies. It should be noted that this approach is less severely affected by the randomizing effects of geometric projections than analyses of the distributions of HI deficiency vs. projected velocity, which have failed to provide any evidence that these two quantities are interrelated (GH85; HG86).

Information on the eccentricity of galaxy orbits can be extracted from the radial run of the line-of-sight (los) velocity dispersion. While the inverse problem of recovering orbital information from radial velocity data only is undetermined, the direct problem is not. Thus, a system with galaxies predominantly in radial orbits necessarily produces an outwardly declining σ_{los} profile. Accordingly, the observation of such a trend in a cluster *is consistent* with radial orbits, while the opposite behavior suggests instead that the galaxy orbits are largely circular. On the other hand, a

roughly constant velocity dispersion with projected radius is characteristic (although not exclusive) of an isotropic distribution of velocities.

We have applied a procedure based on the deconvolution method developed by Sanromá & Salvador-Solé (1989) and Salvador-Solé & Sanromá (1989) to determine the velocity dispersion curves. This technique—which can be used to infer the radial profile of any positive quantity in systems with circular or self-similar symmetry—presents several advantages over the crude annular binning used by Dressler (1986) in his investigation of the orbital parameters of GH85’s galaxies. Among its interesting features are, for instance, its suitability for small samples since the binning of the data is avoided and the fact that it yields a quasi-continuous numerical solution (i.e. known with an arbitrarily small sampling interval). We refer those interested in the fundamentals of this method to the references provided above.

The dependence of the los velocity dispersion on (projected) radius from the cluster center is obtained simply by taking the square root of the ratio of the specific kinetic energy—given by the observed peculiar velocity squared—and the number density profiles of the galaxies. In order to remove from this kinematic profile the disturbing effects of subclustering, each system has been first “circularized” by performing azimuthal scramblings of the observed galaxy positions around the cluster center. In this manner, the distribution of clustercentric distances is preserved, while at the same time any possible subclumps existing in the original structure are destroyed. In addition, the observed peculiar velocities of the galaxies are scaled to the average los velocity dispersion of their parent cluster (see Table 2). This normalization, which is relevant for the composite dataset, has been adopted to give equal weight to identical fractional variations in the velocity dispersion coming from galaxies in different clusters, as well as to avoid artefacts caused by possible fluctuations in the degree of completeness of the galaxy samples according to the clustercentric distance. The mean radial profiles of the normalized los velocity dispersion, σ_{los}^* , for six different galaxian subpopulations, calculated from 100 circularized realizations of the Virgo and composite clusters, are displayed in Figure 12. A low-passband filter with a resolution length of $0.3R_A$ has been applied to each individual simulation to wash out the noise from non-significant statistical fluctuations.

We see in the bottom panel of Figure 12, which depicts the curves corresponding to the composite HI-deficient cluster, that the normalized velocity dispersion for the spirals with the strongest gas deficiencies ($\text{DEF} \geq 0.48$) drops significantly in a manner consistent with radial orbits (see also Dressler 1986). The curve for the gas-rich objects ($\text{DEF} \leq 0$) decreases too with increasing radius—instead of rising as in Dressler’s study—although the decline is sensibly weaker than for the gas-deficient galaxies. These results suggest that one possible explanation for the relationship between disk morphology and gas content (§ 5.1) could be that early spirals have an orbital distribution more radially anisotropic than late types. To test this possibility, we have inferred the velocity dispersion profiles of the spirals subdivided into early and late disks. Again, we find indications of radial orbits for these two broad morphological groupings. However, the trajectories of the galaxies in the first group does not seem to be more eccentric than those in

the second: if anything there is a hint for the opposite effect. Not surprisingly, the kinematic behavior of the entire spiral population is intermediate among those shown by all the previous subdivisions. The lowest curve in the diagram, on the other hand, displays the radial run of the velocity dispersion for the earliest Hubble types, i.e. lenticulars and ellipticals, which have been included in the cluster galaxy samples for this purpose only. These galaxies exhibit a markedly different behavior from the spirals, keeping an almost constant radial profile compatible with an isotropic distribution of velocities. (Recall that the interpretations adopted for the observed trends in the velocity dispersion curves are only valid in the quasi-static cluster interiors.) All these findings are yet another manifestation of the well-known fact that S and E+S0 galaxies do not share the same kinematics: late-type galaxies are likely recent arrivals to the virialized cluster cores, which consist essentially of ellipticals and lenticulars (e.g. Sodr e et al. 1989). In addition to supporting this basic picture, our data also indicate that a segregation develops among the orbits of the infalling spirals according to their gaseous contents since the objects with the more eccentric trajectories, *regardless of morphology*, reach deeper into the cluster cores and are thus more efficiently stripped of their neutral hydrogen.

The same analysis for the Virgo cluster galaxies is reproduced in the top panel of Figure 12. We see that, to a first approximation, the velocity dispersion profiles corresponding to all the different galaxy subgroups are essentially flat (notice, for instance, the curve exhibited by the entire spiral population), although with a noticeably positive excess of the velocity dispersion of the spirals relative to the E+S0 population. As Virgo is still a dynamically young galaxy system (see e.g. Schindler et al. 1999; Gavazzi et al. 1999), we interpret these results as indicative of the fact that the trajectories of the spiral galaxies within the central Virgo region are strongly perturbed by large and rapid fluctuations of the mean gravitational field caused by the ongoing merger of major subclumps. Because of this large-scale phase mixing, environmental influences on the disks have not yet been capable of inducing a neat orbital segregation between gas-poor and gas-rich objects. After this paper was submitted a preprint from Vollmer et al. (2000) became available that investigates, by means of an analytical model of the Virgo cluster, the link between the neutral gas contents of the cluster spirals and their orbits. Their model leads to a scenario in which the majority of HI deficient galaxies of the Virgo centermost region are on radial orbits and have passed through the cluster center at least once. Interestingly enough, the presence of some high-velocity gas-poor objects at relatively large clustercentric distances is interpreted by these authors as a consequence of the perturbations to the main gravitational potential arising from the radial infall of M86 towards M87. These “special” galaxies would result from the spirals that populate the outskirts of the M86 cloud and that, still bound to the system, have been scattered with high velocities to large apocenter orbits during the merger process.

7. Implications of the Results on the Mechanism of HI Depletion

The idea that a spiral galaxy moving through the hot intracluster medium may have its HI removed by ram pressure was first introduced by Gunn & Gott (1972) and has since been extensively invoked. The typical value for the disk restoring force inferred in the solar neighborhood implies that, for ram pressure to be effective, galaxies must pass through or near the cluster cores. Under such circumstances, the low-density HI component can be stripped fairly easily, particularly from the outer disk regions (Abadi, Moore, & Bower 1999). However, the molecular clouds, with densities one million times higher and much lower filling factors, should not be affected. This prediction is in agreement with the observations by Stark et al. (1986) and Kenney & Young (1989) that several HI-deficient Virgo spirals show normal molecular gas contents as indicated by their CO luminosities. Similarly, Kennicutt, Bothun, & Schommer (1984) found that the distribution of $H\alpha$ equivalent widths for spirals in the Cancer, Coma, and A1367 clusters was poorly correlated with the HI content. Truncation of the outer HI disks is also expected from a mechanism in which the local gravity of the galaxy plays an important role in counteracting gas removal. Indeed, the efficiency of ram pressure is regulated by factors such as the mass surface density of the gas and the replenishment rate of the interstellar medium (ISM), related to galaxy type. This complication may well explain our finding that gas deficiency varies with morphology, while it is essentially independent of the size of the stellar disk (§ 5). In this one respect, it is interesting to note that Sb's and earlier spirals often exhibit central HI depressions (Cayatte et al. 1994; Broeils & van Woerden 1994) which, according to recent hydrodynamical treatments of stripping, amplify the effectiveness of this process (Moore, Quilis, & Bower 1999). Thus, it seems reasonable that the strongest deficiencies correspond to the earliest spiral disks.

Observational evidence of ongoing ISM-IGM interactions is provided by galaxies with strongly asymmetric HI distributions (e.g. Dickey & Gavazzi 1991; Bravo-Alfaro et al. 2000). The HI surface-density distributions of these objects show shifts between the optical and 21-cm positions, with extended tails combed backwards from the cluster center and a sharp edge on the forward side, as would be expected from external dynamical pressure effects if the galaxies were currently moving towards the cluster center. In some cases, these asymmetries are associated with radio continuum trails in the same direction as the HI is offset and enhanced star formation on the compressed side of the gas disk (Gavazzi & Jaffe 1987; Dickey & Gavazzi 1991). Often, the interaction of the galaxies with the intracluster medium has been cited as one of the most probable explanations for the presence of blue galaxies with low HI contents in the central portion of some clusters (e.g. Bothun & Dressler 1986). Theoretical studies back up also the plausibility of ram pressure as the physical mechanism behind the change in the star formation rates and colors observed in high-redshift clusters (Fujita & Nagashima 1999), the morphology-density relation of the disk galaxy population in present-day rich clusters (Solanes & Salvador-Solé 1992), and the observed HI deficiency pattern in the Virgo cluster (Vollmer et al. 2000).

Thermal conduction is another IGM-related mechanism capable of producing substantial stripping rates (Nulsen 1982). Its efficiency notwithstanding, this process has longer timescales than

ram pressure and is insensitive to the orbital parameters of the galaxies. In addition, it depends very weakly on the galaxy’s gravity, so it is unlikely that it can generate the observed asymmetries in the HI surface distributions. Galaxy-galaxy interactions (Icke 1985) can also cause important gas depletion, either directly by the tides generated in these encounters or indirectly by inducing star formation. The fact that the galaxy relaxation times are comparable to, or greater than, the age of the universe has led Valluri & Jog (1991) to propose that tidal encounters must occur within subclumps prior to the cluster virialization. Gravitational encounters, however, cannot remove the HI from the inner parts of the galaxies without leaving their imprint on the stars or the molecular component. Model calculations show that tidal effects should produce extended tail structures both in the stellar distribution and in the neutral hydrogen, the latter with surface densities well above the detection threshold of the most sensitive two-dimensional observations. This prediction is at odds with aperture synthesis observations, which show that the HI distributions of cluster galaxies fall off rather rapidly with respect to field galaxies, implying a dearth of atomic gas in the outer parts. The role of gravitational interactions on the morphology of disks—summarized in the modern concept of “galaxy harassment”—has been examined in the context of hierarchical cosmogonies by Moore et al. (1996, 1998). According to their numerical simulations, low surface brightness galaxies can evolve into low luminosity dwarf spheroidals under the influence of rapid tidal encounters with giant galaxies and cluster substructure over a timescale of several billion years. Luminous spirals with large bulges are only affected marginally by this process.

The natural consequence of gas losses as radical as our results indicate would be—provided gas replenishment does not occur at exceptionally high rates—a reduction in the star-formation activity of the galaxy, followed by the fading of the disk. This prediction is in good agreement with the decline of disk luminosity and the invariance of bulge brightness with increasing local density observed in the spirals of rich clusters (Solanes et al. 1989). Also quite consistent with this idea is the finding by Koopmann & Kenney (1998) that objects in Virgo classified as Sa have similar bulge to disk ratios than the Sc’s and only differ in their overall star formation rates which are strongly reduced in the outer disk. The morphological transformation of the swept galaxies into S0-like objects could be completed through the suppression of the spiral features by continued disk heating by tidal encounters, as suggested by Moore et al. (1999). Of course, the possible morphological evolution of cluster spirals towards earlier types has serious difficulties in explaining the presence of S0’s in the field. While some stripped galaxies may have fairly radial orbits that carry them at large distances from the cluster centers, one must bear in mind that not all the lenticular galaxies, outside and inside clusters, arise necessarily from HI-deficient spirals.

We conclude that the present investigation provides clear evidences of the strong influence that the cluster environment has on the gaseous disks of spirals. The marked radial pattern of HI deficiency (§ 3.2) indicates that galaxies lose their gas near the cluster centers. This result is consistent with the finding that spirals with substantial HI deficiency follow orbits with large radial components (§ 6). It appears then, that the stripping of gas requires high IGM densities and relative velocities. According to these results, ISM-IGM interactions, basically ram pressure

supplemented by the accompanying effects of viscosity and turbulence, are favored over other environmental interactions as the main cause of gas depletion in clusters. The existence of very HI-deficient galaxies in the cluster cores, often with deficiency factors of 10 or more (§ 5.1), but that look normal in other aspects (e.g. intrinsic color indices, CO contents), lends weight to the conclusion that the stripping must be relatively recent (probably a few Gyrs ago).

Qualitative support to an IGM-related stripping scenario arises also from the HI deficiency map of the central Virgo region (§ 3.1). The two main subunits of this cluster appear to be in an advanced state of merging, so it is not surprising that their member galaxies, which are moving through the densest portions of the gas sitting on the cluster main potential well, exhibit the highest deficiencies. We have detected also lumps of high HI-deficient galaxies at large projected distances, likely related to secondary galaxy density enhancements and/or background subclumps, which appear to be connected with the cluster center by gas-deficient zones. We speculate that these galaxy aggregates may have already experienced a first high-velocity passage through the Virgo core, that could have affected the gas content of their galaxies and left behind a trail of gas-deficient objects, but that was insufficient to tear apart the densest portions of the lumps. Finally, we want to point out that the two zones having the lowest gas deficiency in our HI-deficiency maps—a small region to the East and South of M49 and a larger one mainly to the South of the M cloud—show a good positional correspondence with two infalling clouds composed almost entirely ($\sim 80\%$) of spirals (Gavazzi et al. 1999).

8. Summary

In this paper, we have used 21-cm-line data to infer the HI contents of 1900 spiral galaxies spanning types Sa to Sdm/Irr in 18 nearby cluster regions. Each galaxy sample is defined by a radial velocity filter of 3σ around the systemic velocity of the central cluster and a projected radius of $5R_A$ around the cluster center, except for the Virgo region, in which we have included only the galaxies located within $3R_A$ of M87.

Following our previous studies, HI deficiency has been quantified by the difference between the observed neutral hydrogen mass and that expected for an isolated galaxy with the same morphological type and linear optical diameter. Improved standards of comparison are taken from the sample of galaxies in low density environments discussed in Paper I. The quality, sensitivity, and large size of the dataset assembled has afforded us the possibility of making—for the first time in a study of these characteristics—an exhaustive, statistically rigorous investigation of the connections between gas deficiency and the properties of both the underlying galaxies and their environment. The main results are:

- Comparison of the distributions of HI content for the spiral population in the inner ($r \leq 1R_A$) and outer ($r > 1R_A$) portions of each cluster field shows that twelve of the systems investigated here—A262, A397, A400, A426, A779, A1060, A1367, Virgo, A1656, A2063, A2147, and

Pegasus—may be considered deficient in HI. Among the non-deficient clusters, three are in the ACO catalog—A539, A3526, and A2151—, while the other three—Pisces, N507, and Cancer—are loosely organized galaxy concentrations.

- The zone of HI paucity can extend out to as much as $2R_A$ from the center of clusters. In the outskirts of these systems, the proportion of gas-deficient objects is compatible with the field values, while in the central cluster regions, HI deficiency is strongly anticorrelated with the projected radial position of the galaxies.
- The total fraction of HI-deficient spirals in a cluster shows no statistically significant trend with other cluster global properties such as X-ray luminosity and temperature, velocity dispersion, richness, or spiral fraction. This result could simply be due to a higher rate of transformation of swept spirals into lenticulars in the richest X-ray clusters. However, possible selection effects and biases propitiated by the small size of some of our cluster galaxy samples make any firm conclusions about this point impossible and demand further investigation with still larger and more complete datasets.
- The amount of gas depletion appears to be related to the morphology of the disks, but it is hardly a function of their optical size. The type dependence is in the sense that both the proportion of gas-deficient objects and the degree of depletion are higher for the early spirals. In the Virgo cluster, where 21-cm observations expand a large range in HI mass, most Sa’s have gas deficiencies exceeding factors of 10, a few being HI poor by more than a factor of 100. The HI deficiency distribution for the Sdm/Irr types in this cluster shows also a heavy tail at the high-deficiency end.
- Orbital segregation of disks according to gas content is observed in HI-deficient clusters: spirals devoid of gas have more eccentric orbits than the gas-rich objects. In the dynamically young Virgo cluster, however, no dependence of the gas deficiency on the orbital parameters of the galaxies is discernible. Collective relaxation effects might be responsible for the spatial pattern of HI deficiency observed in the central Virgo region.

The progressive increase of gas deficiency towards the cluster centers, the eccentricity of the orbits of the gas-poor galaxies, and the 2D pattern of HI deficiency in the central Virgo region, point to a scenario in which gas-sweeping events occur close to the cluster cores where the density of the IGM is highest and the gas-dynamical interactions are strongest. The detection of galaxies with extreme HI deficiencies, but still retaining their spiral morphology, suggests that the stripping of the atomic hydrogen is a relatively recent event in the life of these objects. Furthermore, the details of the relationship between HI deficiency and morphology are consistent with the idea that the presence of central depressions in the HI disks increases the efficiency of gas removal.

We propose that ISM-IGM dynamical interactions are the main agent causing the ablation of the spiral disks in the cluster interiors.

We would like to thank Gregory Bothun for his careful and prompt refereeing which has led to a much-improved presentation of the paper. J. M. S. would like also to express his gratitude to Eduardo Salvador-Solé for many fruitful discussions and the Departament d’Astronomia i Meteorologia at the Universitat de Barcelona for its generous hospitality. J. M. S., A. M., C. G. G., and G. G. C. acknowledge support by the Direcció General de Investigació Científica y Tècnica, under contracts PB96–0173 and PB97–0411. Partial support has also been provided by US NSF grants AST–9528860 to M. P. H., AST–9617069 to R. G., and AST–9900695 to M. P. H. and R. G.

REFERENCES

- Abadi, M. G., Moore, B., & Bower, R. G. 1999, *MNRAS*, 308, 947
- Abell, G. O., Corwin, H. G. Jr., & Olowin, R. P. 1989, *ApJS*, 70, 1 (ACO)
- Abramopoulos, F., & Ku, W. H. M. 1983, *ApJ*, 271, 446
- Bahcall, N. A. 1977, *ApJ*, 218, L93
- Balogh, M. L., Navarro, J. F., & Morris, S. L. 2000, preprint (astro-ph/0004078)
- Balogh, M. L., Schade, D., Morris, S. L., Yee, H. K. C., Carlberg, R. G., & Ellingson, E. 1998, *ApJ*, 504, L75
- Beers, T. C., Gebhardt, K., Huchra, J. P., Forman, W., Jones, C., & Bothun, G. D. 1992, *ApJ*, 400, 410
- Binggeli, B., Popescu, C., & Tammann, G. A. 1993, *A&AS*, 98, 275
- Böhringer, H., Briel, U. G., Schwarz, R. A., Voges, W., Hartner, G., & Trümper, J. 1994, *Nature*, 368, 828
- Bothun, G. D., & Dressler, A. 1986, *ApJ*, 301, 57
- Bothun, G. D., Geller, M. J., Beers, T. C., & Huchra, J. P. 1983, *ApJ*, 268, 47
- Bothun, G. D., Schommer, R. A., & Sullivan, W. T. 1984, *AJ*, 89, 466
- Bravo-Alfaro, H., Cayatte, V., van Gorkom, J. H., & Balkowski, C. 2000, *AJ*, 119, 580
- Broeils, A., & van Woerden, H. 1994, *A&AS*, 107, 129
- Carlberg, R. G., Yee, H. K. C., & Ellingson, E. 1997, *ApJ*, 478, 462
- Cayatte, V., Kotanyi, C., Balkowski, C., & van Gorkom, J. H. 1994, *AJ*, 107, 1003
- Chamaraux, P., Balkowski, C., & Fontanelli, P. 1986, *A&A*, 165, 15

- David, L. P., Slyz, A., Jones, C., Forman, W., Vrtillek, S. D., & Arnaud, K. A. 1993, *ApJ*, 412, 479
- Davis, R. D., & Lewis, B. M. 1973, *MNRAS*, 165, 231
- de Vaucouleurs, G., & de Vaucouleurs, A. 1973, *A&A*, 28, 109
- Dickey, J. M., & Gavazzi, G. 1991, *ApJ*, 373, 347
- Dressler, A. 1980, *ApJ*, 236, 351
- Dressler, A. 1986, *ApJ*, 301, 35
- Edge, A. C., & Stewart, G. C. 1991, *MNRAS*, 252, 428
- Fadda, D., Girardi, M., Giuricin, G., Mardirossian, F., & Mezzetti, M. 1996, *ApJ*, 473, 670
- Fitchett, M., & Merrit, D. 1988, *ApJ*, 335, 18
- Fujita, Y., & Nagashima, M. 1999, *ApJ*, 516, 619
- Gavazzi, G., Boselli, A., Scodreggio, M., Pierini, D., & Belsole, E. 1999, *MNRAS*, 304, 595
- Gavazzi, G., & Jaffe, W. 1987, *A&A*, 186, L1
- Ghigna, S., Moore, B., Governato, F., Lake, G., Quinn, T., & Stadel, J. 1998, *MNRAS*, 300, 146
- Giovanardi, C., Helou, G., Krumm, N., & Salpeter, E. E. 1983, *ApJ*, 267, 35
- Giovanelli, R., Chincarini, G. L., & Haynes, M. P. 1981, *ApJ*, 247, 383
- Giovanelli, R., & Haynes, M. P. 1983, *AJ*, 88, 881
- Giovanelli, R., & Haynes, M. P. 1985, *ApJ*, 292, 404 (GH85)
- Giovanelli, R., Haynes, M. P., Salzer, J. J., Wegner, G., Da Costa, L. N., & Freudling, W. 1994, *AJ*, 107, 2036
- Guiderdoni, B. 1987, *A&A*, 172, 27
- Guiderdoni, B., & Rocca-Volmerange, B. 1985, *A&A*, 151, 108
- Gunn, J. E., & Gott, J. R. 1972, *ApJ*, 176, 1
- Haynes, M. P., & Giovanelli, R. 1984, *AJ*, 89, 758 (HG84)
- Haynes, M. P., & Giovanelli, R. 1986, *ApJ*, 306, 466 (HG86)
- Helou, G., Giovanardi, C., Salpeter, E. E., & Krumm, N. 1981, *ApJS*, 46, 267
- Hoffman, G. L., Helou, G., & Salpeter, E. E. 1988, *ApJ*, 324, 75

- Horner, D. J., Mushotzky, R. F., & Scharf, C. A. 1999, *ApJ*, 520, 78
- Icke, V. 1985, *A&A*, 144, 115
- Jones, C., & Forman, W. 1984, *ApJ*, 276, 38
- Jones, C., & Forman, W. 1999, *ApJ*, 511, 65
- Kenney, J. D. P., & Young, J. S. 1989, *ApJ*, 344, 171
- Kennicutt, R. C., Bothun, G. D., & Schommer, R. A. 1984, *AJ*, 89, 1279
- Koopmann, R. A., & Kenney, J. D. P. 1998, *ApJ*, 497, 75
- Magri, C., Haynes, M. P., Forman, W., Jones, C., & Giovanelli, R. 1988, *ApJ*, 333, 136
- Moore, B., Katz, N., Lake, G., Dressler, A., & Oemler, A. Jr. 1996, *Nature*, 379, 613
- Moore, B., Lake, G., & Katz, N. 1998, *ApJ*, 495, 139
- Moore, B., Quilis, V., & Bower, R. 1999, in *ASP Conf. Ser. 197, Dynamics of Galaxies: from the Early Universe to the Present*, ed. F. Combes, G. A. Mamon, & V. Charmandaris (San Francisco: ASP), 363
- Nilson, P. 1973, *Uppsala General Catalog of Galaxies* (Uppsala: Astr. Obs. Pub.) (UGC)
- Nulsen, P. E. J. 1982, *MNRAS*, 198, 1007
- Quintana, H., & Melnick, J. 1982, *AJ*, 87, 972
- Ramírez, A. C., & de Souza, R. E. 1998, *ApJ*, 496, 693
- Salvador-Solé, E., & Sanromá, M. 1989, *ApJ*, 345, 660
- Sanromá, M., & Salvador-Solé, E. 1989, *ApJ*, 342, 17
- Schindler, S., Binggeli, B., & Böhringer, H. 1999, *A&A*, 343, 420
- Sodré, L. Jr., Capelato, H. V., Steiner, J. E., & Mazure, A. 1989, *AJ*, 97, 1279
- Solanes, J. M., Giovanelli, R., & Haynes, M. P. 1996, *ApJ*, 461, 609 (Paper I)
- Solanes, J. M., & Salvador-Solé, E. 1992, *ApJ*, 395, 91
- Solanes, J. M., Salvador-Solé, E., & Sanromá, M. 1989, *AJ*, 98, 798
- Stark, A. A., Knapp, G. R., Bally, J., Wilson, R. W., Penzias, A. A., & Rowe, A. E. 1986, *ApJ*, 310, 660
- Stauffer, J. R. 1983, *ApJ*, 264, 14

- Strubble, M. F., & Rood, H. J. 1991, *ApJS*, 77, 363
- Sullivan, W. T., Bothun, G. D., Bates, B., & Schommer, R. A. 1981, *AJ*, 86, 919
- Valluri, M., & Jog, C. J. 1991, *ApJ*, 374, 103
- van den Bergh, S. 1976, *ApJ*, 206, 883
- Vollmer, B., Cayatte, V., Balkowski, C., & Duschl, W. J. 2000, *ApJ*, in press
- Warmels, R. H. 1986, Ph. D. Thesis, University of Groningen
- Warmels, R. H. 1988a, *A&AS*, 72, 19
- Warmels, R. H. 1988b, *A&AS*, 72, 57
- White, D. A., Jones, C., & Forman, W. 1997, *MNRAS*, 292, 419
- Zabludoff, A. I., Geller, M. J., Huchra, J. P., & Vogeley, M. S. 1993, *AJ*, 106, 1273

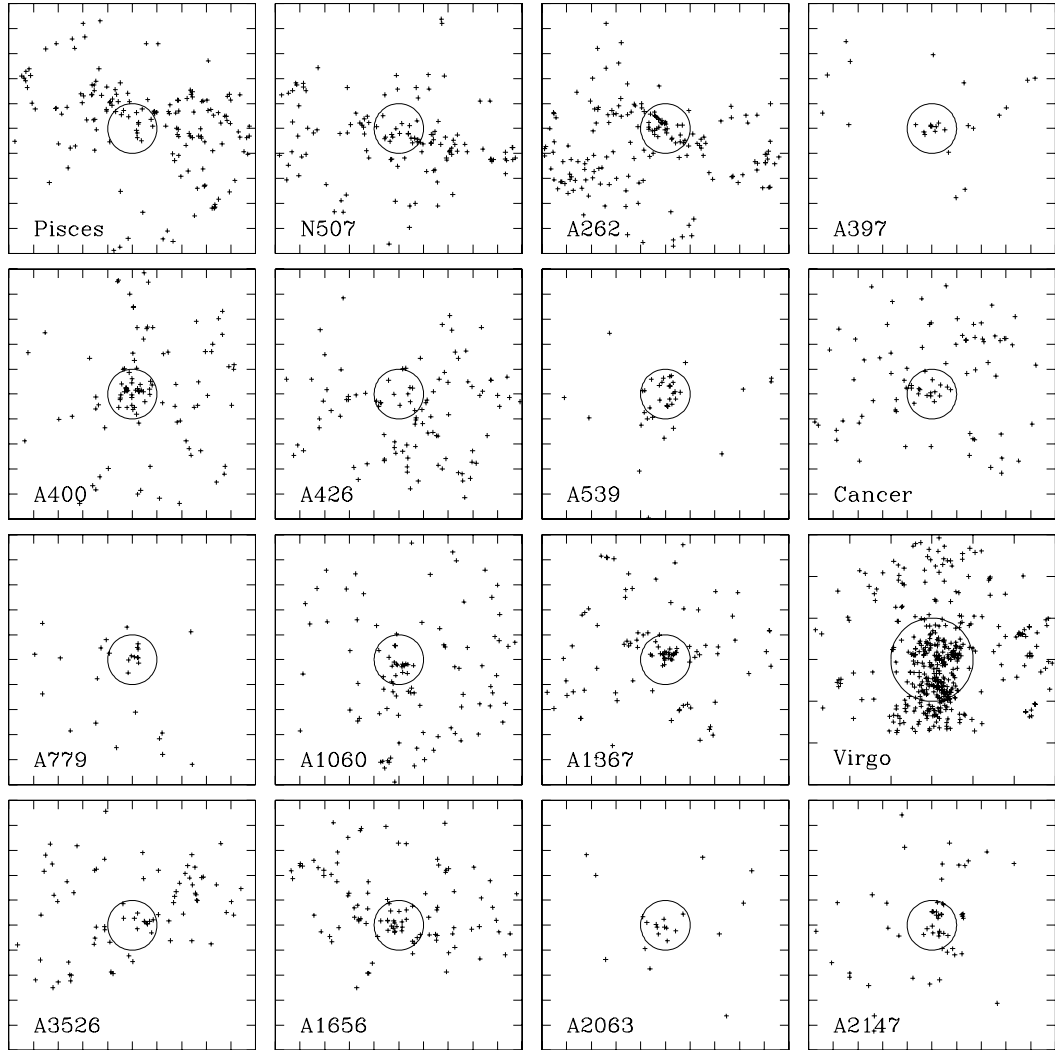


Fig. 1.— Sky distribution of spirals with good HI deficiency measures in each one of our eighteen nearby cluster fields. Tickmarks are in units of Abell radii. The circle superposed on each panel encompasses the objects located within the innermost $1R_A$ region.

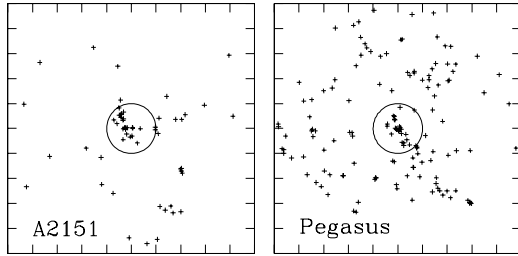


Fig. 1.— Continued.

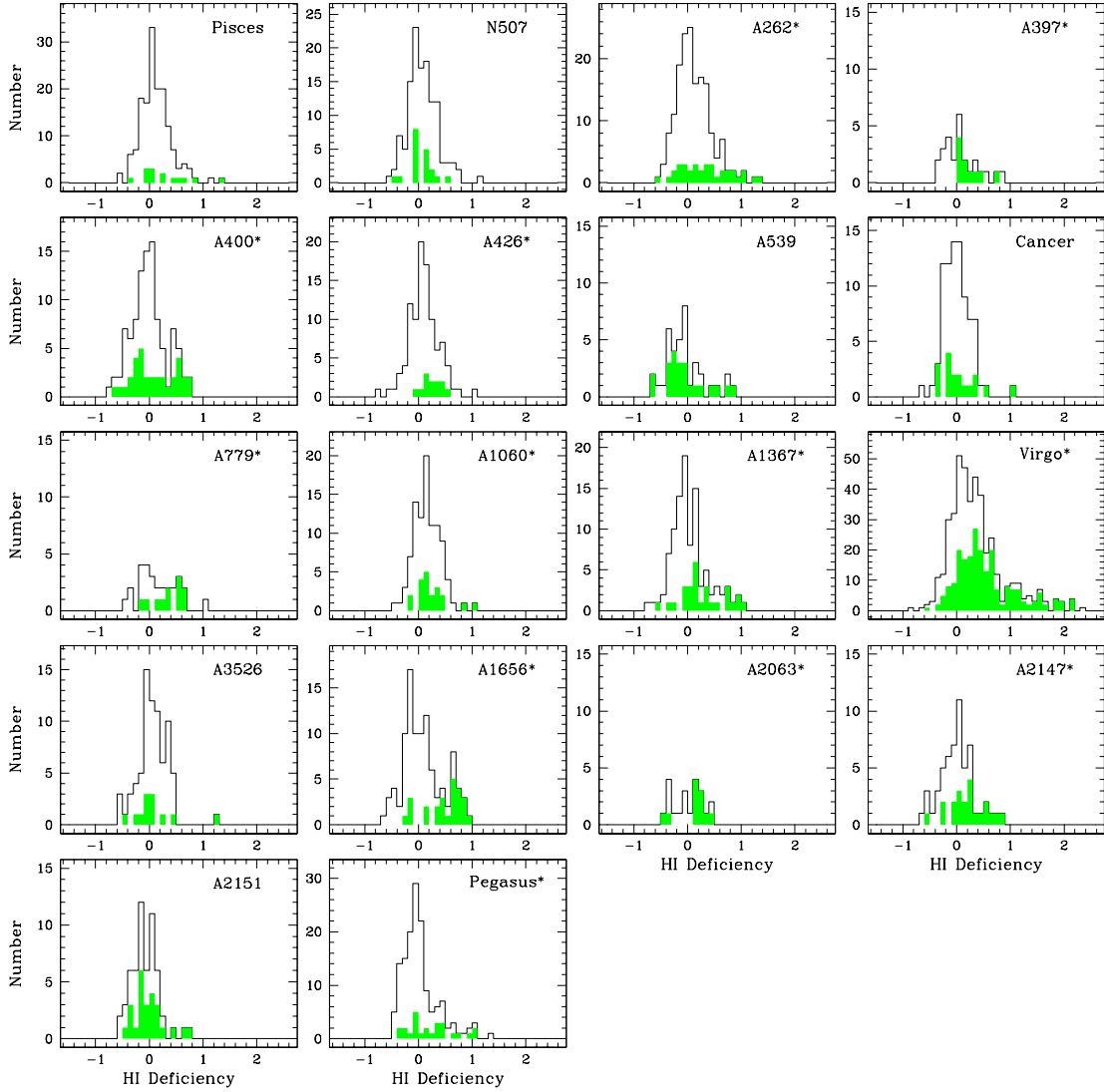


Fig. 2.— Histograms showing the distribution of the computed HI deficiency parameter DEF for each cluster region. In each panel the filled portions of the histogram indicate deficiencies for galaxies located within $1R_A$ of the cluster center, while the unfilled areas represent galaxies at larger radii: up to $3R_A$ for the Virgo field and up to $5R_A$ for the remaining cluster regions. HI-deficient clusters (identified by an asterisk after the name) are those for which a Kolmogorov-Smirnov test finds less than 10% probability that the inner and outer distributions of DEF are drawn from the same parent population.

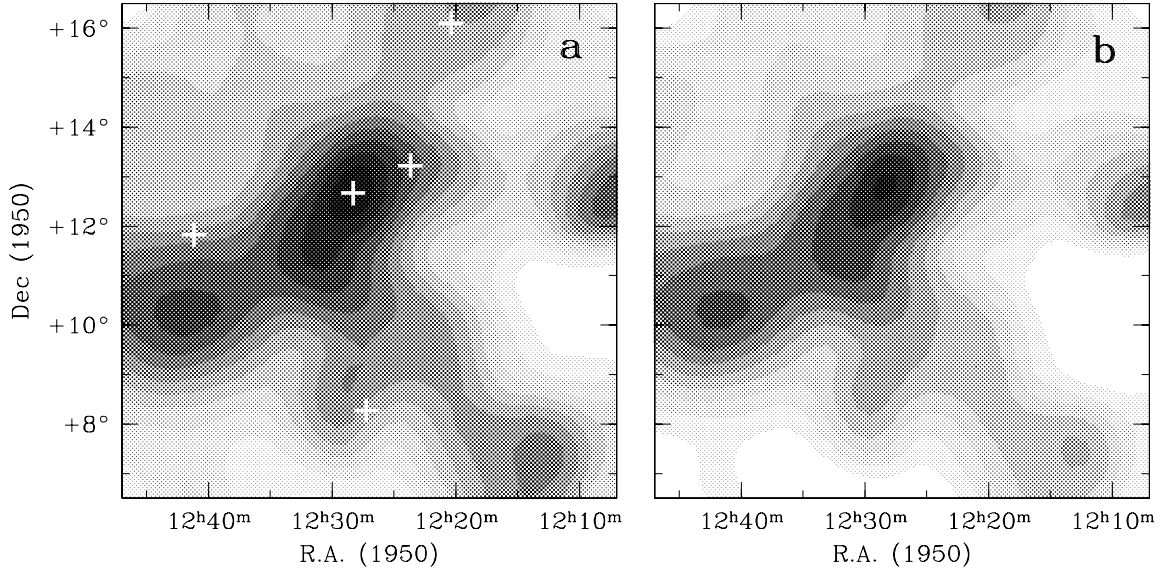


Fig. 3.— Greyscale images of the sky distribution of the HI deficiency in the central region of the Virgo cluster: (a) using the HI deficiency parameter DEF, and (b) a distance-independent approximation of it (see text). The lightest regions in the maps correspond to $\text{DEF} < 0.1$ and the darkest to $\text{DEF} \geq 1.2$. The contour spacing is linear. The peak value of HI deficiency is located near the position of M87, which coincides with the maximum of X-ray emission in the whole area. The positions of five dominant galaxies are marked by crosses (top to bottom: M100, M86, M87, M60, and M49). The size of the images is $10^\circ \times 10^\circ$.

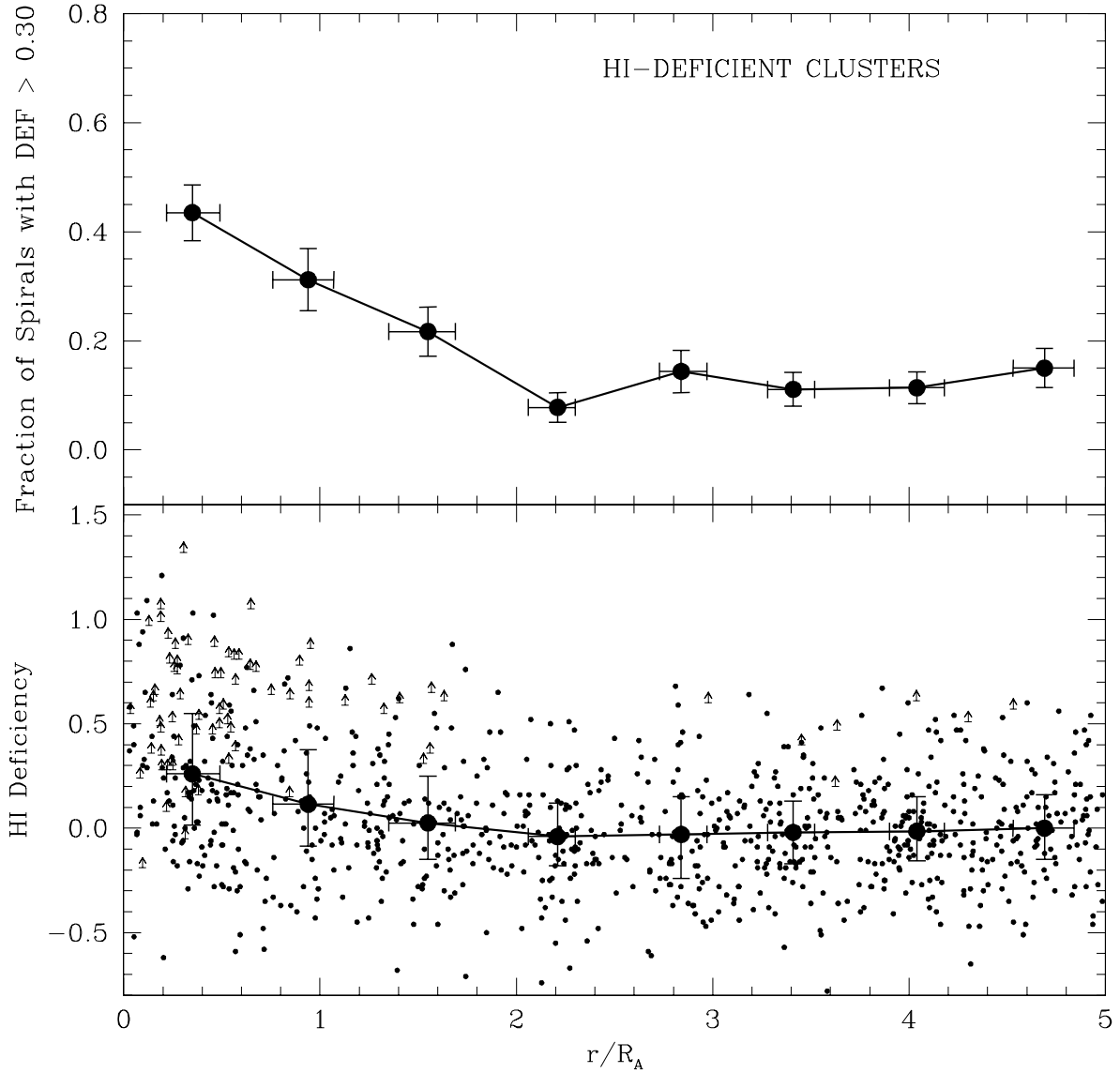


Fig. 4.— *Top*: HI-deficient fraction in bins of projected radius from the cluster center for the superposition of all the HI-deficient clusters but Virgo. Vertical error bars correspond to 1σ confidence Poisson intervals. The abscissas show medians and quartile values of the bins in radial distance. *Bottom*: same in upper panel for the measured HI deficiency. Displayed are the medians and quartiles of the binned number distributions in HI deficiency. Small dots show the radial variation of HI deficiency for individual galaxies while the arrows identify non-detections plotted at their estimated lower limits.

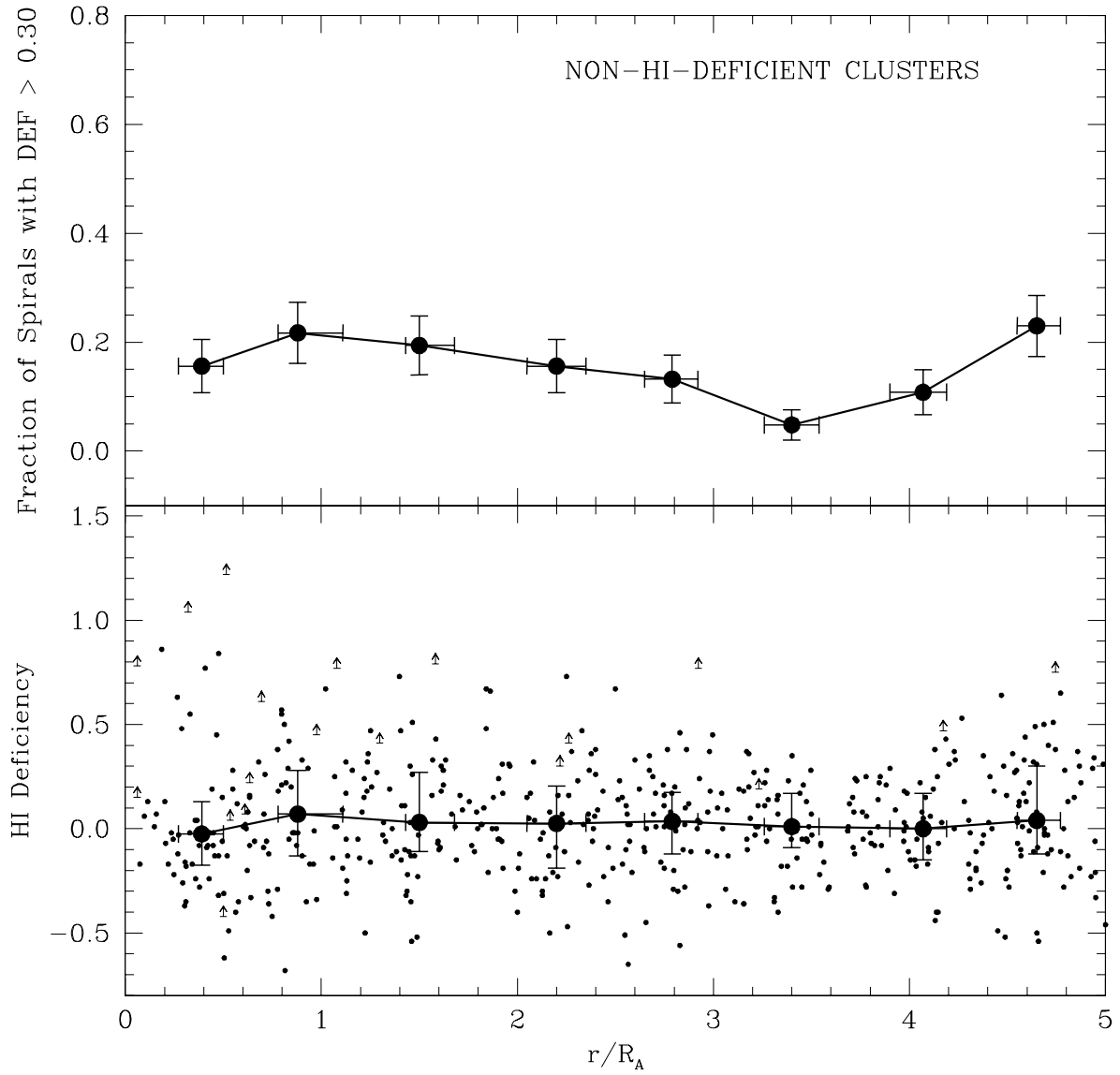


Fig. 5.— Same as in Fig. 4 but for the superposition of all the non-HI-deficient clusters.

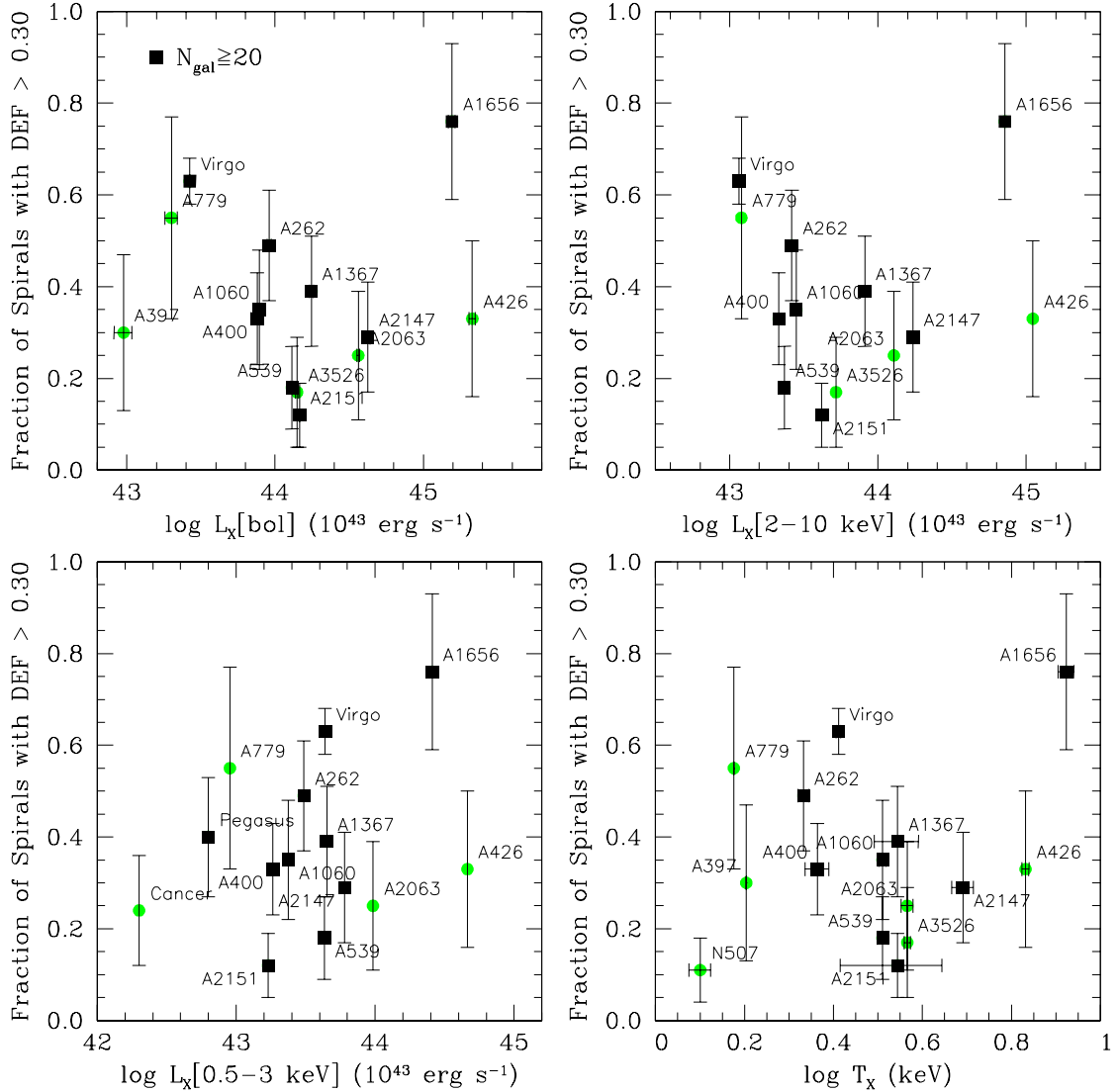


Fig. 6.— From left to right and top to bottom, spiral fraction within $1R_A$ with a deficiency parameter DEF larger than 0.30 vs. cluster bolometric, 2–10 keV, and 0.5–3.0 keV X-ray luminosities, and cluster X-ray temperature. Square symbols identify clusters with a minimum of 20 objects in the central region. Vertical error bars correspond to 1σ Poisson confidence intervals, except for the temperature where the quoted uncertainties are 90% for the ASCA observations and 68% for the *Einstein* estimates (see Table 2).

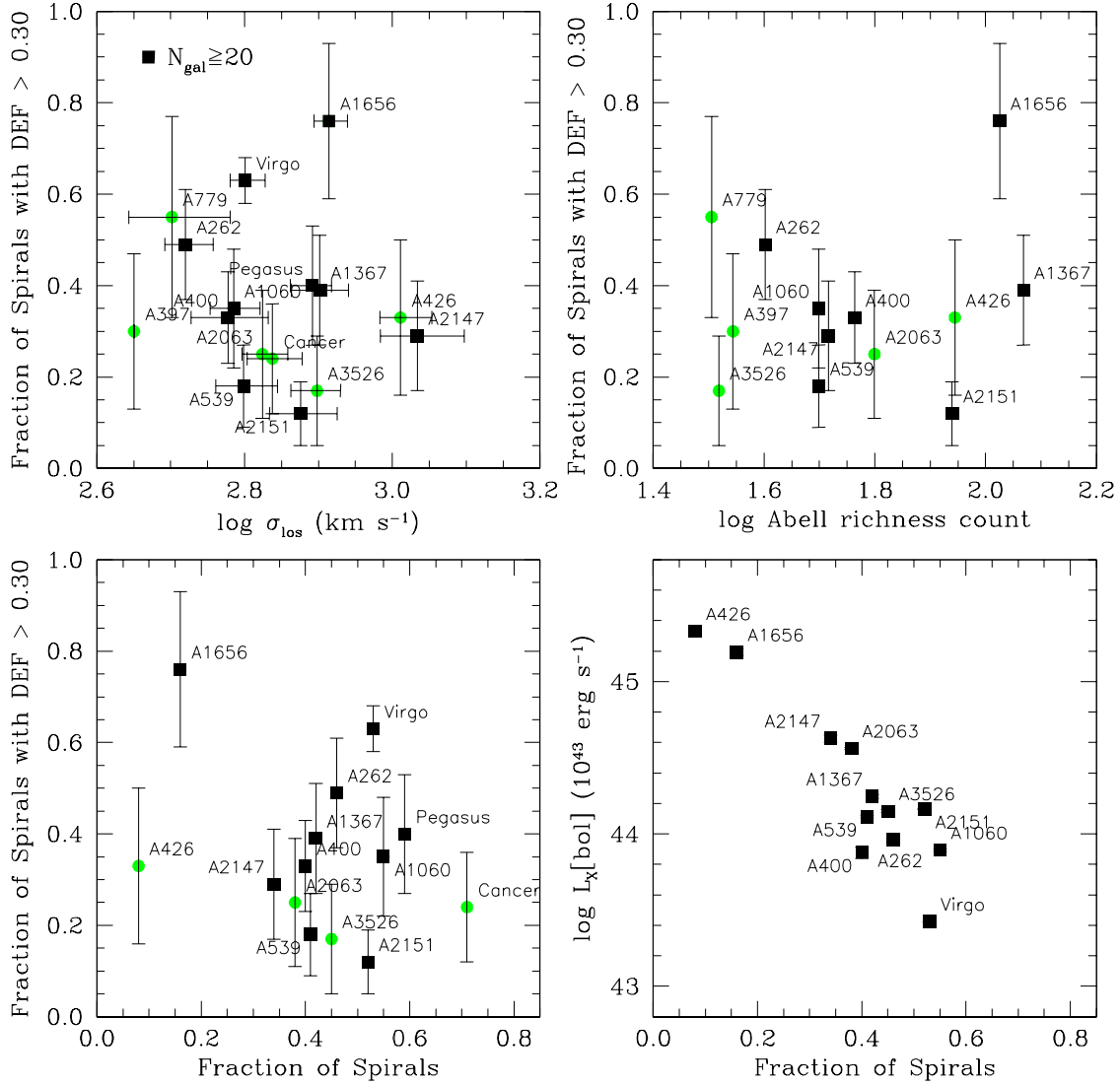


Fig. 7.— From left to right and top to bottom, spiral fraction within $1R_A$ with a deficiency parameter DEF larger than 0.30 vs. cluster velocity dispersion, Abell richness count, and total fraction of spirals. The bottom right panel shows the bolometric X-ray luminosity plotted against the total fraction of spirals. Vertical error bars correspond to 1σ confidence intervals. In the bottom right panel the size of the symbols is larger than the error bars.

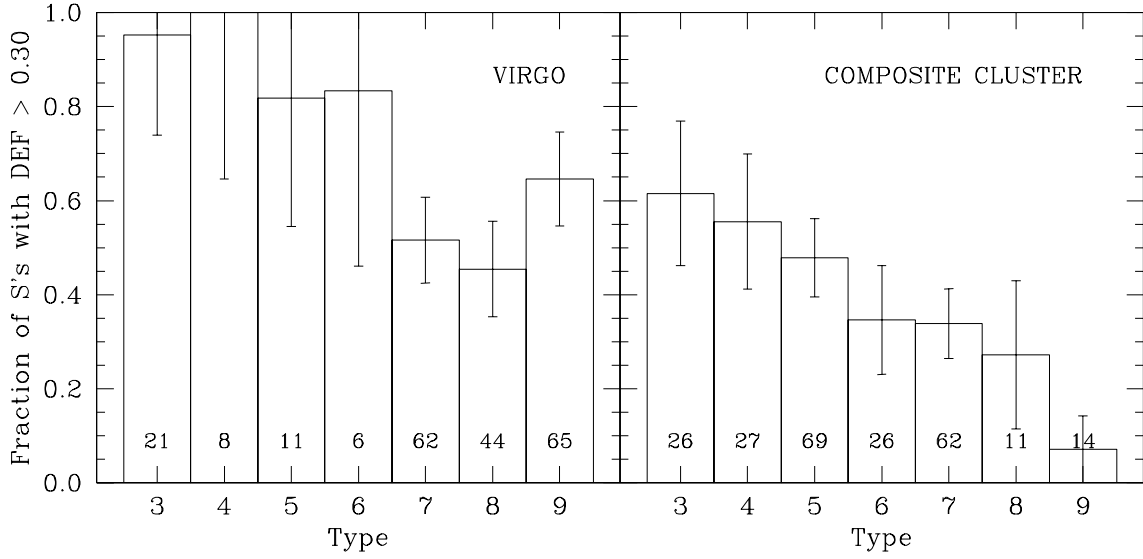


Fig. 8.— Fraction of galaxies within $1R_A$ with deficiency parameter $DEF > 0.30$ as a function of the morphological type (Sa–Sdm/Irr) for the Virgo sample (left) and a composite cluster sample formed by combining the rest of the HI-deficient systems (right). The numbers within each bin indicate the total number of galaxies in that bin. Error bars correspond to 1σ Poisson errors.

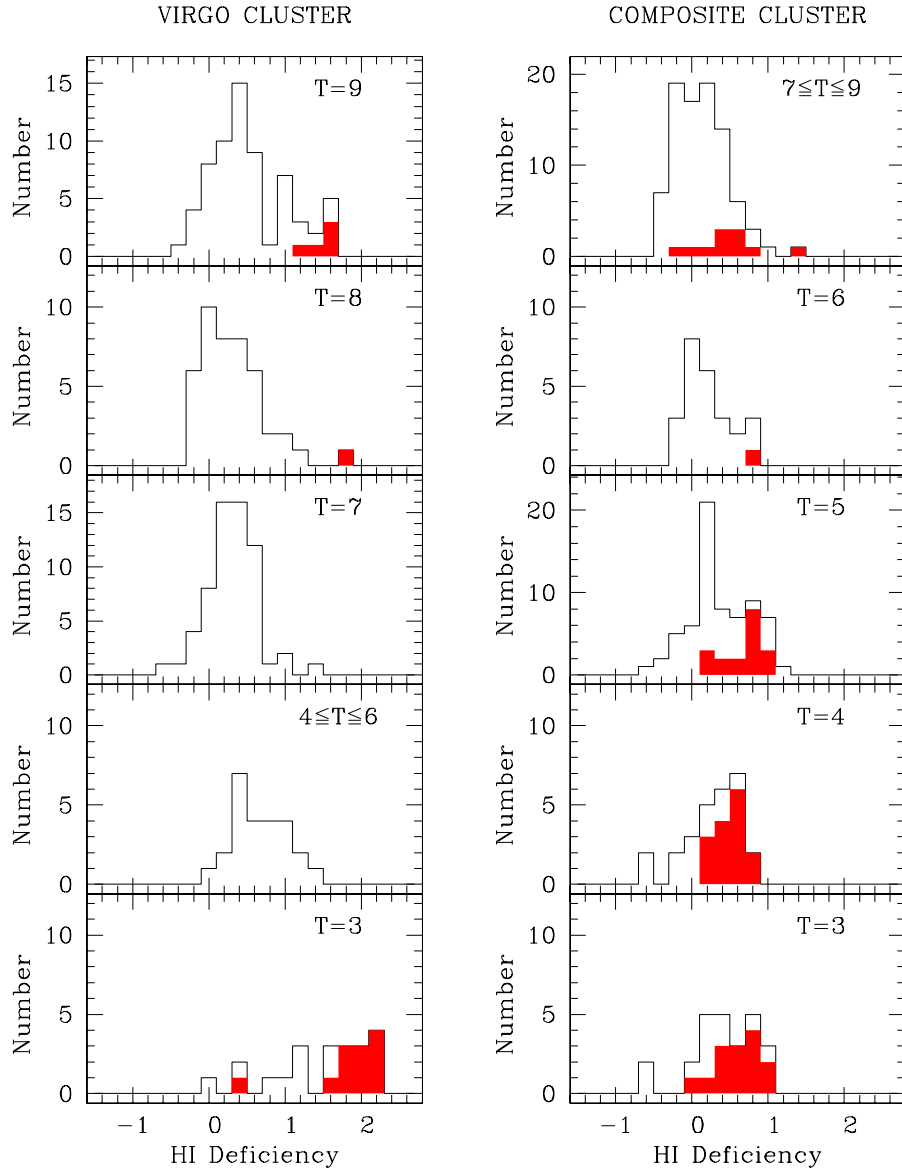


Fig. 9.— HI deficiency histograms of the spirals lying within $1R_A$ of the Virgo (*left*) and the composite HI-deficient cluster (*right*) centers separately by morphological type. In each panel the dark portions of the histograms correspond to those galaxies undetected in HI for which a lower limit on HI deficiency has been estimated. Non-detections contribute with their nominal lower limits of deficiency.

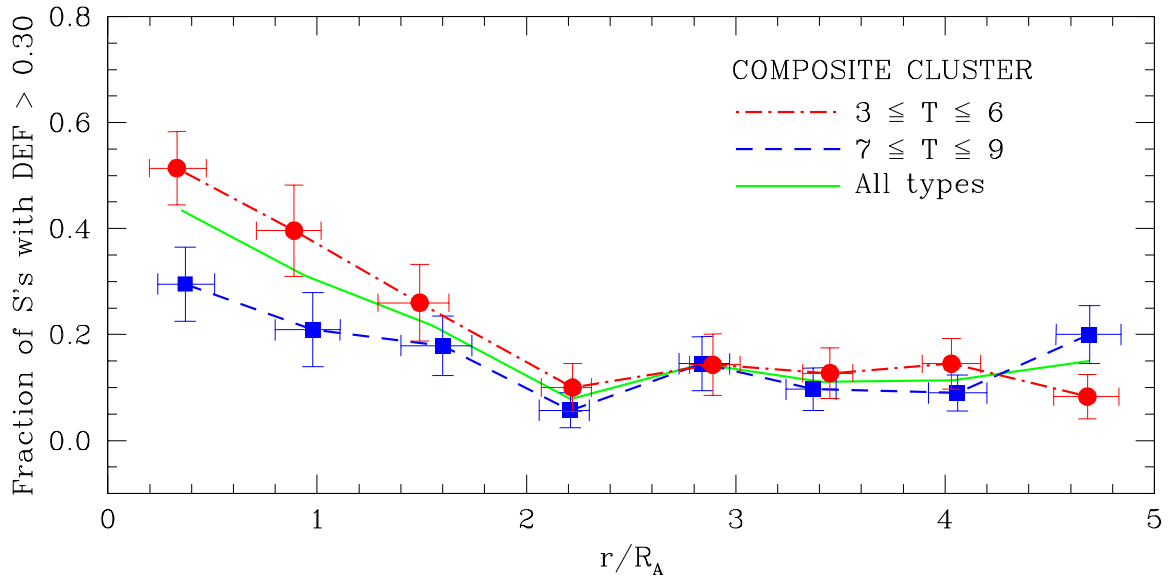


Fig. 10.— Same as in the upper panel of Fig. 4, for the early (circles) and late (squares) spirals separately. The solid curve reproduces the trend of the entire spiral population. Only error bars for the two morphological subgroups are displayed for clarity.

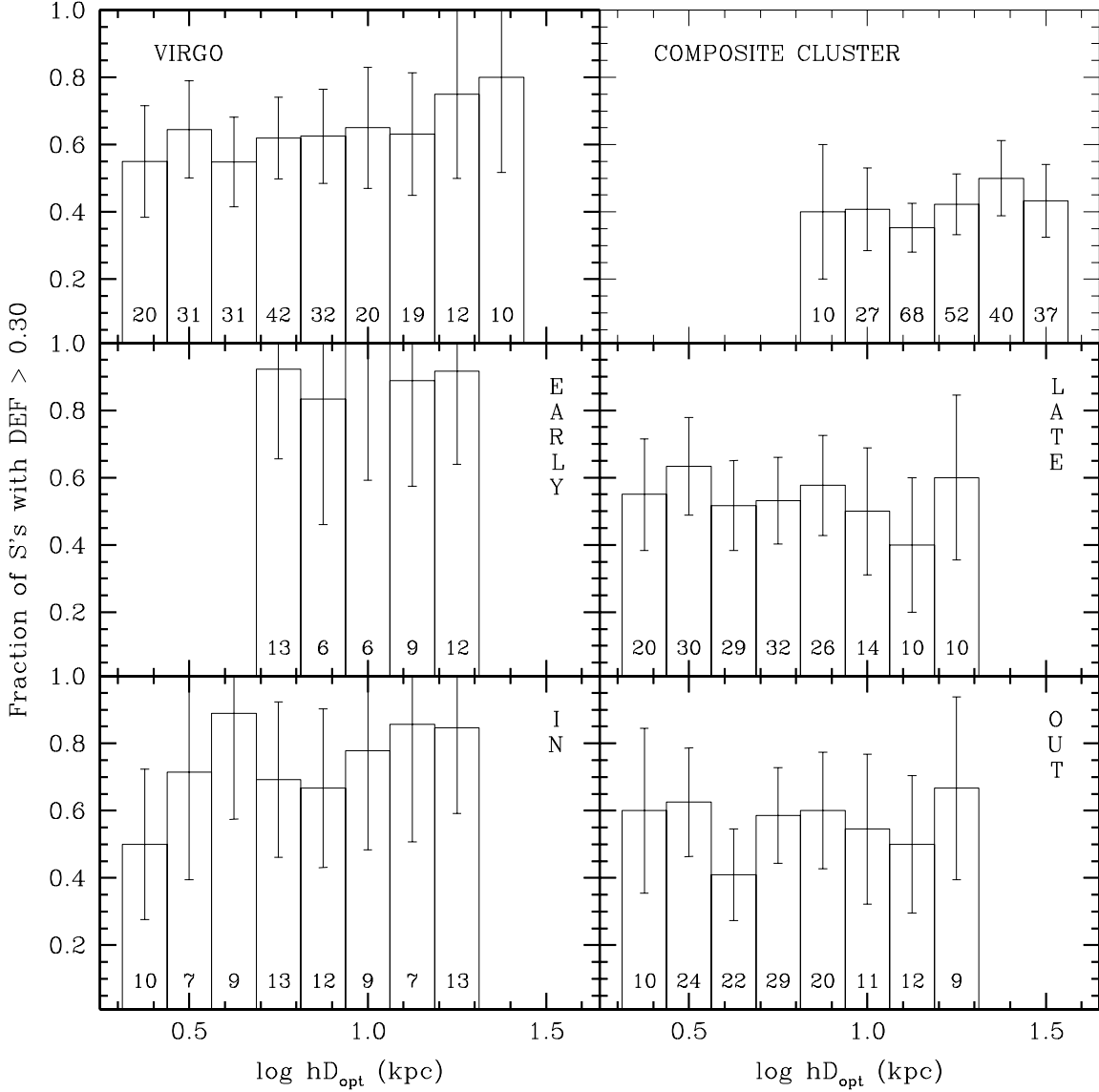


Fig. 11.— *Top*: Spiral fraction within $1R_A$ with $DEF > 0.30$ as a function of the linear optical diameter for the Virgo (left) and the composite HI-deficient cluster (right). *Middle*: Same as in the upper left panel but separately for the early (left) and late (right) spiral subsets. *Bottom*: Same as in the upper left panel but separately for the subsets of galaxies located within $0.5R_A$ from M87 (left) and beyond this distance (right). The numbers within the bars indicate the galaxies in each bin. In all panels the few galaxies with sizes outside the plotted range have been accumulated in the extremal bins to avoid large statistical fluctuations. Error bars correspond to 1σ Poisson errors.

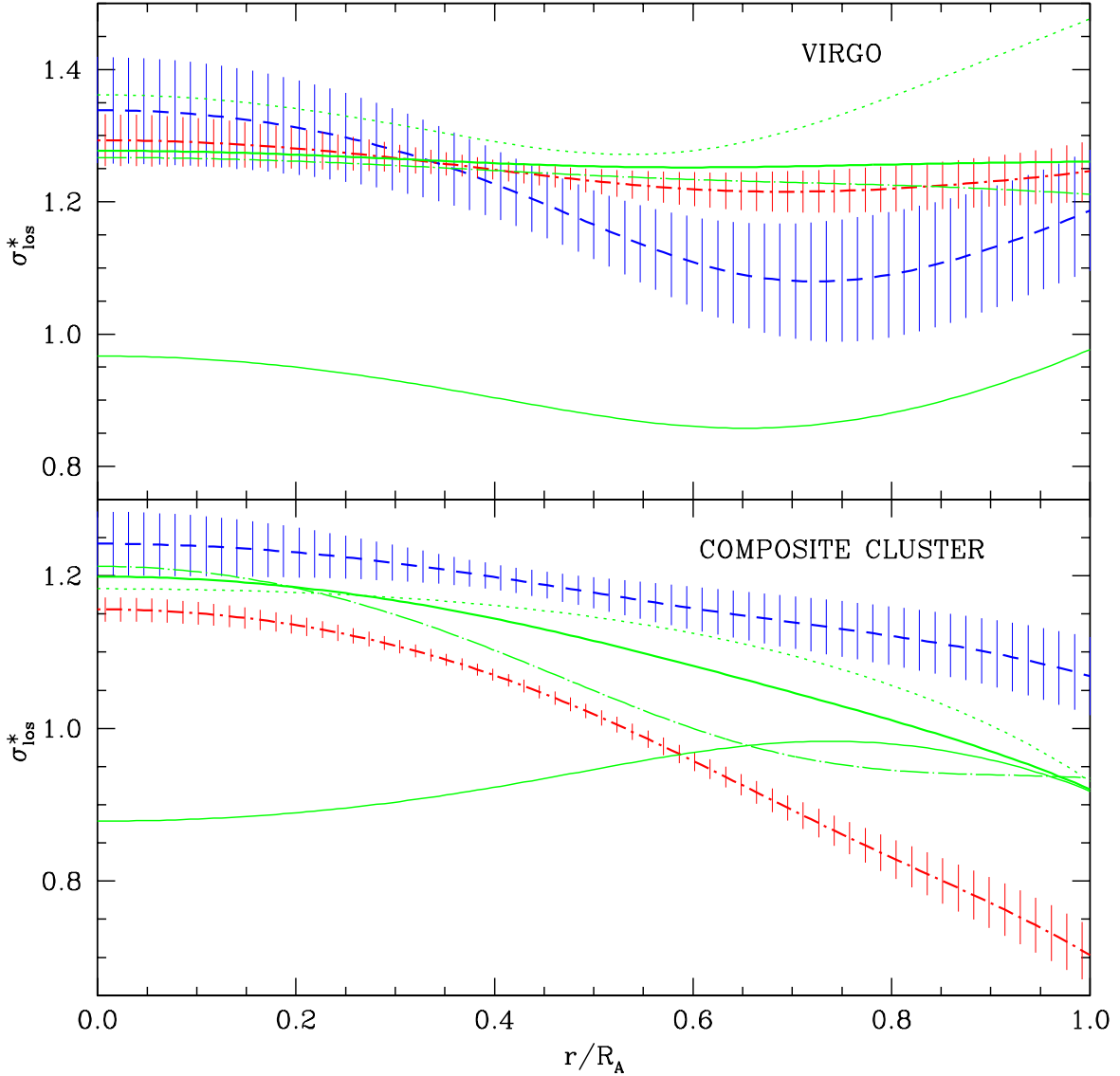


Fig. 12.— Radial run of the *normalized* los velocity dispersion up to $1R_A$ for the Virgo (top) and the composite HI-deficient cluster (bottom). Line coding is as follows: thick dot-dash for spirals with $DEF \geq 0.48$, thick dash for spirals with $DEF \leq 0$, thick solid for all spirals, dots for early spirals, dot-long dash for late spirals, and solid for ellipticals and lenticulars. In both plots vertical error bars correspond to 1σ confidence intervals. Only error bars for the profiles corresponding to the spirals with extremal HI contents are displayed for clarity.

Table 1. List of Cluster Fields

Name (1)	R.A. (1950)			Dec. (1950)			Velocity Filter (km s ⁻¹) (4)	R_A (deg) (5)	# of Galaxies		P_{KS} (8)
	(h)	(m)	(s)	(°)	(')	(")			$r \leq 1R_A$ (6)	$r \leq 5R_A^a$ (7)	
Pisces	00	59	54.0	+30	02	00	3500÷7500	1.88	14	155	0.316
N507	01	24	26.8	+34	03	35	3500÷7500	1.83	19	124	0.497
A262	01	49	49.9	+35	53	50	3000÷7000	1.90	35	168	0.002
A397	02	53	51.2	+15	41	35	8500÷11000	0.95	10	26	0.003
A400	02	55	00.0	+05	48	25	5000÷9000	1.28	33	100	0.057
A426	03	16	30.0	+41	20	00	2000÷9000	1.70	12	99	0.008
A539	05	13	55.2	+06	23	16	6500÷10500	1.03	22	38	0.909
Cancer	08	17	00.0	+21	11	00	2500÷7000	1.75	17	83	0.581
A779	09	16	44.3	+33	57	18	4500÷9000	1.25	11	28	0.012
A1060	10	34	27.7	-27	16	26	2000÷5500	2.16	20	96	0.060
A1367	11	42	04.6	+19	59	14	4000÷9000	1.32	28	100	<0.001
Virgo	12	28	18.0	+12	40	00	-500÷2700	7.23	218	426	<0.001
A3526	12	46	06.0	-41	02	00	1400÷4500	2.54	12	76	0.491
A1656	12	57	18.3	+28	12	22	4000÷10000	1.25	25	100	<0.001
A2063	15	20	39.1	+08	47	18	9000÷12000	0.84	11	21	0.004
A2147	15	59	58.3	+16	06	15	8000÷14000	0.86	21	57	0.002
A2151	16	02	22.0	+17	51	48	8000÷14000	0.82	25	58	0.405
Pegasus	23	18	00.0	+07	55	00	2000÷5500	2.36	25	145	0.011

^aThe maximum radial cutoff for the Virgo cluster is $3R_A$.

Table 2. Global Properties of Clusters

Name	$L_X(\text{bol})^a$	$L_X(\text{soft})^b$	$L_X(\text{hard})^c$	T_X^d	σ_{los}^e	C^f	F_S^g	F_{DEF}
(1)	(2)	(3)	(4)	(5)	(6)	(7)	(8)	(9)
Pisces	0.36 ± 0.16
N507	1.26 ± 0.07	0.11 ± 0.07
A262	9.15 ± 0.30	3.07	2.63	2.15 ± 0.06	525^{+47}_{-33}	40	0.46	0.49 ± 0.12
A397	0.95 ± 0.13	1.60	447	35	...	0.30 ± 0.17
A400	7.56 ± 0.65	1.84	2.14	2.31 ± 0.14	599^{+80}_{-65}	58	0.40	0.33 ± 0.10
A426	214.0 ± 10.3	46.1	111	6.79 ± 0.12	1026^{+106}_{-64}	88	0.08	0.33 ± 0.17
A539	13.00 ± 0.28	<4.30	2.34	3.24 ± 0.09	629^{+70}_{-52}	50	0.41	0.18 ± 0.09
Cancer	...	<0.20	688^{+67}_{-52}	...	0.71	0.24 ± 0.12
A779	2.00 ± 0.19	<0.90	<1.20	1.50	503^{+100}_{-63}	32	...	0.55 ± 0.22
A1060	7.81 ± 0.18	2.37	2.81	3.24 ± 0.06	610^{+52}_{-43}	50	0.55	0.35 ± 0.13
A1367	17.60 ± 0.52	4.49	8.15	3.50 ± 0.40	798^{+75}_{-68}	117	0.42	0.39 ± 0.12
Virgo	2.66	4.37	1.16	2.58 ± 0.03	632^{+41}_{-29}	...	0.53	0.63 ± 0.05
A3526	14.10 ± 0.32	...	5.21	3.68 ± 0.06	791^{+60}_{-62}	33	0.45	0.17 ± 0.12
A1656	156.0 ± 8.30	25.7	71.9	8.38 ± 0.34	821^{+49}_{-38}	106	0.16	0.76 ± 0.17
A2063	36.40 ± 0.66	9.65	12.8	3.68 ± 0.11	667^{+55}_{-41}	63	0.38	0.25 ± 0.14
A2147	42.30 ± 2.32	6.03	17.2	4.91 ± 0.28	1081^{+170}_{-117}	52	0.34	0.29 ± 0.12
A2151	14.6	1.70	4.18	3.50 ± 0.90	751^{+91}_{-69}	87	0.52	0.12 ± 0.07
Pegasus	...	<0.63	780^{+47}_{-52}	...	0.59	0.40 ± 0.13

^aBolometric X-ray luminosities primarily from White, Jones, & Forman (1997). The value for Virgo comes from David et al. (1993).

^b*Einstein* X-ray luminosities in the 0.5–3 keV energy range from Jones & Forman (1984) and GH85. Upper limits for A539 and A779 are from Abramopoulos & Ku (1983).

^cX-ray luminosities in the 2–10 keV energy range primarily from the compilation of *Einstein*, *Exosat*, and *Ginga* data by David et al. (1993). The upper limit for A779 comes from Quintana & Melnick (1982).

^dX-ray temperatures primarily from the compilation of ASCA observations by Horner, Mushotzky, & Scharf (1999). For A397, A779, A1367, and A2151, we use *Einstein* estimates from White et al. (1997).

^eCluster radial velocity dispersions primarily from Fadda et al. (1996). Values for A779 and A2147 have been drawn from Zabludoff et al. (1993), and for A397 from Strubble & Rood (1991). Cancer was observed by Bothun et al. (1983).

^fAbell richness count inside $1R_A$ from Abell et al. (1989).

^gFraction of spirals from averages of the values listed in Bahcall (1977), Dressler (1980), and GH85.